Journal of Petroleum Science and Engineering 191 (2020) 107136

Contents lists available at ScienceDirect

Journal of Petroleum Science and Engineering

journal homepage: http://www.elsevier.com/locate/petrol

Cuttings transport: On the effect of drill pipe rotation and lateral motion on the cuttings bed

Alexander Busch [a,*], Stein Tore Johansen [a,b]

[a] Norwegian University of Science and Technology (NTNU), Trondheim, Norway
[b] SINTEF Industry, Trondheim, Norway

ARTICLE INFO

Keywords:
Cuttings transport
Hole cleaning
Drilling
CFD
Rotation
Whirling
Orbital motion

ABSTRACT

Drill pipe rotation is considered a relevant factor for cuttings transport and hole cleaning. However, in the term "rotation" is often used as a moniker for the combination of plain drill pipe rotation around its own axis and more complex lateral motion, as many laboratory setups feature an unconstrained drill string. Lateral motion is generally considered to benefit the transports of cuttings due to increased bed agitation. By means of Computational Fluid Dynamics, we have investigated the effect of synchronous and asynchronous whirling drill string motion on the cuttings bed and cuttings transport for water and a more viscous, shear-thinning fluid using the Two Fluid Model in conjunction with the Kinetic Theory Of Granular Flows and closures from soil mechanics to rheologically describe granular matter. The dynamic mesh capability of ANSYS Fluent R17.2 is exploited to account for the orbital motion of the drill string. In addition, three base cases (negative eccentric, concentric, and positive eccentric) are investigated for comparison. Whirling motion helps tremendously to disperse the solids into the main flow region and hence improves the quality of cuttings transport and hole cleaning, with synchronous whirl by far outperforming asynchronous whirl due to the cumulative tangential and radial velocities. The effect is much more prominent for water than for the more viscous, shear-thinning fluid because the latter already shows a comparatively good cuttings transport performance. Moreover, in case of the more viscous, shear-thinning fluid, the positive eccentric annulus provides an even better cuttings transport capability, if comparison is made on equivalent pressure gradients. Because of the higher viscosity level, the whirling motion reduces the axial throughput, which despite the increased bed agitation results in worse performance compared to the positive eccentric case.

1. Introduction

In petroleum drilling, solid particles (cuttings) are generated by the drill bit which is being pushed downhole with a certain rate of penetration (ROP). The cuttings are subsequently transported by the often shear-thinning drilling fluid through the annular space (created by the drill pipe[1] in a wellbore) to the surface, as qualitatively depicted in Fig. 1.

Adequate cuttings transport is required for proper hole cleaning, i.e. the absence of a critical cuttings bed to avoid costly downtimes in drilling due to e.g. stuck pipes. The quality of solids transport depends on many factors (A. Busch et al., 2018a, Busch et al., 2019), two of which are drill pipe rotation and eccentricity. Due to the relevance of cuttings transport to the drilling industry, these have been the subject of many experimental studies (Avila et al., 2008; e.g. Han et al., 2010; Larsen, 1990; Sanchez et al., 1999; Tomren et al., 1986) over the last decades as well as numerical, or more precisely Computational Fluid Dynamics (CFD) studies (e.g. Akhshik et al., 2015; Epelle and Gerogiorgis, 2017; Heydari et al., 2017; Pang et al., 2019, 2018) in recent years.

1.1. Effect of parameters on cuttings transport and hole cleaning

Negative[2] eccentricity increases the accumulation of particles at the

* Corresponding author.
E-mail addresses: alexander.busch@ntnu.no, alexander.busch@alumni.ntnu.no (A. Busch).

[1] Strictly speaking, one needs to distinguish between individual drill pipe elements and the drill string made up of several drill pipe elements. However, for simplicity and because we here focus on an annular element with length L < 10 m, we use the terms interchangeably.

[2] The coordinate system employed in this study is depicted in Fig. 1 and defined as follows: Assuming a horizontal wellbore, i.e. an inclination of 90° as used in the petroleum industry, the streamwise direction is positive x, the vertical direction against gravity is positive y, and the direction out of the plane is positive z. Thus, negative eccentricity is characterizing a drill pipe out-of-center towards the lower side of the annulus, whereas positive eccentricity is the opposite.

https://doi.org/10.1016/j.petrol.2020.107136
Received 19 June 2019; Received in revised form 26 February 2020; Accepted 28 February 2020
Available online 4 March 2020

Nomenclature

Greek symbols

α	Volume fraction
γ	Shear rate, total shear measure
Δ	Difference
ε	Turbulent dissipation rate
η	Apparent shear viscosity
κ	Bulk viscosity
μ	Newtonian shear viscosity
ω	Specific turbulent dissipation rate
ϕ	Inclination
φ	Angle of internal friction
Π	Non-dimensional quantity
ρ	Density
σ	Prandtl number
τ	Deviatoric stress tensor
θ	Circumferential coordinate
Θ	Granular temperature

Latin symbols

A	Surface area, Amplitude
c	Coefficient
d	Diameter, Differential
D	Rate of deformation tensor
e	Non-dimensional eccentricity, coefficient of restitution
E	Dimensional eccentricity
f	Functional
f	Force vector
g	Radial distribution function
g	Gravity
I	Identity tensor
k	Turbulent kinetic energy, Granular conductivity
K	Power-law parameter (also known as Consistency Index), interphase exchange coefficient
l	Limiter coefficient
L	Length
m	Mass
n	Parameter in Power-law (PL), also known as PL exponent
N	Normal stress difference
p	Pressure
Q	Volumetric flow rate
Re	Reynolds number
r	Radial, Rock
t	Time.
T	Relaxation time.
Ta	Taylor number
T	Stress tensor
u	Phase velocity
U	Fluid bulk velocity
v	Particle velocity
V	Volume
w	Width
x	Spatial dimension
y	Spatial dimension
z	Spatial dimension

Indices

0	Zero, $\gamma \to 0$
∞	Infinity, $\gamma \to \infty$
c	Collisional
D	Drag
f	Fluid, Frictional
i, j,k	Index
i	Inner
j	Joint
k	Kinetic
MR	Metzner-Reed
o	Outer
p	Pipe.
PL	Power Law
r	Relative.
s	Solid, Slip (Subscript), Superficial (Superscript)
t	Turbulent
T	Transposed.
VM	Virtual mass
w	Whirl

Abbreviations

2D, 3D	Two-, Three dimensional in space
AW	Asynchronous Whirl
BC	Boundary Condition
CFD	Computational Fluid Dynamics
CMC	Sodium Carboxymethyl Cellulose
CTR	Cuttings Transport Ratio
DEM	Discrete Element Method
FC	Flow Curve
GNF	Generalized Newtonian Fluid
HB	Herschel-Bulkley
KTGF	Kinetic Theory of Granular Flows
MP	Multi-Phase
PAC	Polyanionic Cellulose
PL	Power-Law
RPM	Revolutions Per Minute
ROP	Rate Of Penetration
SP	Single-Phase
SST	Shear Stress Transport
SW	Synchronous Whirl
TFM	Two Fluid Model

lower side of the annulus (leading to a sediment or cuttings bed) because the narrower gap results in a local reduction in fluid velocity (Bicalho et al., 2016a; Heydari et al., 2017). At the same time, pressure loss decreases because the effective cross-sectional flow area increases. This also holds for the single-phase (SP) case, regardless of fluid type or flow regime (McCann et al., 1995). Rotation on the other hand generally increases the transport of cuttings (Duan et al., 2010; Han et al., 2010), in particular in the cases off negative eccentric configurations because the tangential velocity of the rotating pipe is acting at the position of high solid volume fractions, i.e. at the cuttings bed (Bicalho et al., 2016a; Heydari et al., 2017; Xiaofeng et al., 2014). However, this effect is dependent on the particle size as small particles will be re-entrained much easier than large ones (Duan et al., 2008; Sifferman et al., 1992) as well as the annular diameter ratio, as the effect of rotation becomes much more relevant for smaller annular gaps (Peden et al., 1990). By reducing an existing cuttings bed and thereby increasing the effective flow area, drill pipe rotation leads to a decrease in pressure loss, which is different to the SP case where rotation may increase or decrease pressure losses, depending on the flow regime and fluid (Sorgun et al., 2011). For instance, pressure losses increase with rotation for turbulent flows and decrease for laminar flows of Power-Law (PL) fluids because of the shear-thinning property of the fluid (Johansen et al., 2003; McCann

et al., 1995). On the other hand, for the case of Yield-Power-Law (YPL)/Herschel-Bulkley (HB) fluids, Erge et al. (2015, 2014) observed no significant effect of rotation for turbulent flows and a pressure loss increase or decrease in the laminar and transitional regime, depending on the magnitude of inertial forces, i.e. the spatial dimensions of the annulus as well as the viscosity level of the fluid.

Often, in cuttings transport studies, the drill string is assumed to rest in a fixed position, which may be either concentric or eccentric. However, this is rarely the case in wellbores (Ahmed et al., 2010; Saasen, 2014), where the drill pipe may feature complex lateral motion patterns (Gao, 2010; Leine et al., 2002; Shyu, 1989). Rotation is a necessary requirement for lateral motions. For a given rate of rotation, a variety of lateral motion patterns may be observed depending on the three-dimensional (3D) wellbore trajectory and the particular point of the wellbore one focuses on. The flexibility of the drill pipe (Xiao et al., 2003) and the buckling of the drill string (Erge et al., 2015, 2014), as a consequence of the axial force applied on the string and the bit, i.e. weight on bit, determine the local eccentricity and in combination with the drill string rotation and its experienced torque (Leine et al., 2002) as well as the hydrodynamic pressure and viscous forces of the drilling fluid (Leine et al., 2002; Xiao et al., 2003) lead to a specific lateral motion.

In general, a drill pipe rotating in a wellbore with an angular velocity $\omega p = 2\pi$ rpmp/60 may feature a variety of lateral/orbital motion patterns, which include the absence of lateral motion, i.e. pure rotation, snaking motion, where the drill pipes climbs the annular wall to a certain extent and then falls back due to gravity, irregular motion, and whirling motion, where the drill pipe rolls or slides on the surface of the outer pipe in an clockwise or anti-clockwise manner, as detailed further in section 2.1 (Gao, 2010).

While specific types of lateral motion of the drill string may cause material wear and damage (Cayeux et al., 2018) as well as an increase in average pressure drop (Erge et al., 2015, 2014; Khatibi et al., 2018a, 2018b) and pressure oscillations (Khatibi et al., 2018a), it is also reasonable to expect an increased transport of cuttings because the motion of the drill pipe additionally agitates the bed and entrains particles into the bulk of the liquid flow. However, only a very limited number of research activities have focused on the specific effect of lateral drill string motion on cuttings transport.

1.2. State of the art of lateral drill string motion experiments

In experimental studies, both rotation and eccentricity have been extensively investigated and in many laboratory setups rotation and eccentricity are truly independent parameters (e.g. Duan et al., 2010; Peden et al., 1990; Sifferman et al., 1992). However, in many other laboratories (e.g. Avila et al., 2008; Khatibi et al., 2018a, 2018b; Sanchez et al., 1999; Sayindla et al., 2017; Ytrehus et al., 2018, 2015) the drill string is not entirely constrained and hence lateral, orbital and/or whirling motion may occur. Thus, the eccentricity at the point of observation is time-dependent and a function of the aforementioned parameters and, unfortunately, often undisclosed.

In a review conducted by Pilehvari et al. (1999), the relevance of the role of lateral drill pipe motion is first mentioned as "the manner in which the drill string behaves dynamically" and attributed to the study of Bassal (1996) in the sense that "all previous experimental studies had limitations in simulating the real dynamics of the drill pipe". At the same time, many of these results were disseminated by Sanchez et al. (1999).

In the experiments of Sanchez et al. (1999), the drill string was only constrained at its end and hence was able to move freely in the middle where flow observations were made. Sanchez et al. (1999) showed that not the pure rotation but rather the resulting orbital motion is the reason for significant improvement of hole cleaning, both during actual drilling and after drilling when cuttings generation has ceased.

1.3. State of the art of lateral drill string motion modelling

Recently, Computational Fluid Dynamics (CFD) has been increasingly used to study wellbore flows (e.g. Bicalho et al., 2016a; Bilgesu et al., 2002; Epelle and Gerogiorgis, 2017; Hajidavalloo et al., 2013; Heydari et al., 2017; Mme and Skalle, 2012; Ofei et al., 2014; Ofei and Pao, 2014; Pang et al., 2018, 2019; Pereira et al., 2007; Rooki et al., 2013a, 2013b; Wang et al., 2009; Xiaofeng et al., 2014). Typically, rotation is treated as plain drill string rotation and simply accounted for by specifying a tangential no-slip velocity at the drill pipe wall. The role of whirling motion, however, has gained much less attention.

Very recently, Pang et al. (2019) studied orbital drill pipe motion by means of CFD for the case of a PL fluid and showed that orbital motion increases the cuttings transport ratio (CTR) while decreasing the pressure drop (However, higher rotating speeds cause a sharp increase in pressure drop in particular when the drill pipe orbits in the opposite direction to its self-rotation). The larger the radius of the orbital motion, the better for the CTR. Orbital motion periodically stirs up the cutting bed by causing the core zone of the axial bulk velocity following the orbital motion (though lagging behind that) and producing secondary tangential flows and eddies. Pang et al. (2019) utilized the Eulerian-Eulerian Two Fluid Model (TFM) in combination with the Kinetic Theory of Granular Flows (KTGF), though no additional closures were employed to account for frictional effects within the dense granular media, i.e. the cuttings bed. The sliding mesh method of ANSYS Fluent R14.0 was employed to realize the orbital motion of the drill pipe. Self-rotational speed ωp and orbital speed ωw were considered to be equivalent in magnitude, i.e. $\omega w = \omega p$ and $\omega w = -\omega p$, and investigated in the range 0–200 rpm.

Recently, Cayeux et al. (2018) investigated the special case of

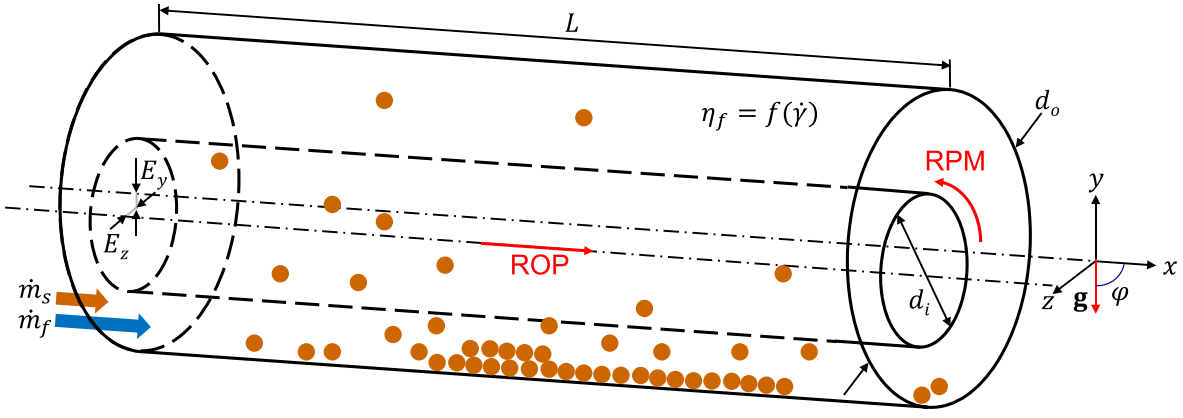

Fig. 1. Cuttings transport process on an annular scale.

synchronous whirl, where the drill string angular frequency equals the angular frequency of the whirling motion and the pipe always faces the same side towards the outer wall of the annulus, comprising the cases of SP laminar flow of Newtonian, PL, and HB fluids. Based on the methodology used by Feng et al. (2007) they inverted the annular system by considering the outer cylinder rotating around the inner and accounted for centrifugal and Coriolis forces. The whirling motion contributes to the total pressure gradient for all fluids investigated. However, in case of the HB fluid the pressure gradient of the pure rotational cases exceeds the one of the whirling cases at approximately 80 rpm for all volumetric flow rates investigated, presumably because the whirling motion avoids plug regions at higher rotational speeds (Cayeux et al., 2018).

Both Vieira Neto et al. (2012) and (Bicalho et al., 2016b, 2016a) experimentally investigated the flow of laminar xanthan gum solutions in annuli with orbital inner pipe motion. In addition, they simulated the pressure drop using the dynamic meshing (Neto et al., 2012) and sliding mesh capabilities (Bicalho et al., 2016a, 2016b) of ANSYS Fluent and obtained a good fit between experimental and numerical results. Rotation and corresponding orbital motion of the inner tube results in more uniform flow distributions in the annulus, preventing flow stagnation in the narrow-gap regions in cases of eccentric configurations. Therefore, in the case of a partially blocked annulus with eccentricity, increasing drill pipe rotation and orbital motion is considered to improve the transport of cuttings (Bicalho et al., 2016a).

For a negative eccentricity of a highly shear thinning fluid, Demiralp (2014) investigated the effect of different whirl patterns on cuttings transport. A two-way coupling between solids and fluid by means of CFD and the Discrete Element Method (DEM) and presumably (The details of the whirling motion implementation are not disclosed) the dynamic meshing capabilities of ANSYS Fluent were employed to investigate hole cleaning for different fluid superficial velocities and drill pipe rotations. Solids concentration decreases with increasing whirling speed in all flow regimes, with synchronous whirl yielding the highest solid superficial velocity.

1.4. Purpose, scope and structure of this paper

While some numerical studies investigated the impact of whirling motion on the flow hydrodynamics (Bicalho et al., 2016a; Cayeux et al., 2018; Feng et al., 2007; Neto et al., 2012), the effect of drill pipe whirl on cuttings transport has—to our knowledge—not been quantitatively investigated, with the notable exceptions of the thesis of Demiralp (2014) and the recent study of Pang et al. (2019). Experimental investigations have often featured a laterally moving drill string; however, the lateral motion is usually a consequence of the system and the controlling parameter is simply the rotational rate of the drill pipe. Unfortunately, no clear distinction is made in the literature between plain drill pipe rotation and additional lateral, orbital, or whirling motion, in particular when it comes to the interpretation and quantification of experimental results. Even recent review papers combine these under the umbrella rotation (Kelin et al., 2013; Li and Luft, 2014a, 2014b; Ofei et al., 2015; Xiaofeng et al., 2013). In addition, we are not aware of any study where the modes of and the parameters describing orbital motion were disseminated. This hinders quantitative comparisons.

We numerically investigate the effect of two classical whirling motion cases, namely forward and backward whirl (detailed definitions are provided in the following section 2.1), on cuttings transport for water and a more viscous, shear-thinning fluid. We then compare these results to eccentric and concentric cases with plain drill string rotation.

In the following section, a description of the drill string whirl cases as well as all relevant other parameters investigated is presented, followed by a brief summary of the physical CFD model along with required closures. SP results are then presented and compared to the experiments of Khatibi et al. (2018a, 2018b), followed by the presentation of cuttings transport simulation results. In the subsequent discussion, we provide explanations for the observed phenomena as well as an analysis of the strength and weaknesses of our investigations. Finally, a brief summary and outlook is given.

2. Materials and Methods

2.1. Drill string whirl

In general, four patterns of drill pipe motion may be characterized as follows (Shyu, 1989):

1. Synchronous whirl (SW), also known as forward whirl, where the tool joint is sliding on the hole/casing wall in such a manner that it always faces the same side towards the outer wall. Consequently, the drill pipe rotation and its whirling motion show identical angular velocities, i.e. ωw = ωp.
2. Asynchronous whirl (AW), also known as backward whirl, where the tool joint is rolling on the hole/casing wall without any slip. Consequently, the whirling motion occurs in opposite direction of the drill pipe rotation and the angular velocity of the whirl motion is given by ωw = -dj/doωp, where dj is the diameter of the tool joints.
3. More complex whirl, where there is slip between the surfaces such that ωw = csωp, where cs is different from 1 or -dj/da, not necessarily constant and may even be different for the y and z-direction such that the motion pattern becomes a Lissajou curve.
4. Any other (seemingly chaotic) motion, where e.g. the drill string does not always remain in contact with the wellbore wall (at all times) and/or where there is slip between the surfaces of tool joints and wellbore wall.

We here focus on plain whirling motion, i.e. type 1 and 2 as characterized above, because it is easiest to parametrize. A generic framework for the whirling motion is given by a 2D oscillation equation in y and z:

$$y_w = (E_y + A_y) - A_y \cos(\omega_y t), \tag{1}$$

$$z_w = E_z + A_z \sin(\omega_z t), \tag{2}$$

where Ei are the dimensional eccentricities, Ai the dimensional amplitudes, and ωi the angular velocities (which are here taken as ωw = ωy = ωz), as depicted in Fig. 2.

While SW and AW may be straightforwardly parametrized as described above, this is not so in many experimental setups because the drill string is free to move in the test section. For instance, in the experiments of Khatibi et al. (2018a, 2018b), the eccentricity and amplitude are functions of the drill pipe's rotation rate and the superficial fluid velocity. The drill pipe consisted of several acrylic elements connected with flexible joints, the diameter of which was slightly larger than the drill pipe (see Fig. 17 in Appendix C). One end was connected to a dual current motor while the other end was not constrained and hence free to move. Therefore, the flexible drill string arrangement was subject to lateral motion because of the enforced rotation at one end and the systems mechanical properties (compliances of individual drill string elements and flexible joints, Coulomb and viscous friction). Khatibi et al. (2018b) showed, that in their SP experiments the observed change in vertical eccentricity Ey is largely dependent on the rotation rate of the drill pipe and to a smaller extent on the Reynolds number of the flow. We curve-fitted second-order polynomials to the available dimensional data (Khatibi, 2018), the coefficients of which are presented in Table 1.

In the experiments of Khatibi et al. (2018a, 2018b), the horizontal amplitude Az as well as the angular velocity ω_w were not determined explicitly. However, the latter may be estimated with $2\pi\, rpm/60$ based on the frequency spectra analysis of pressure readings (Khatibi, 2018; Khatibi et al., 2018a), while the former may be roughly estimated by $A_y/2$ (Khatibi, 2018).

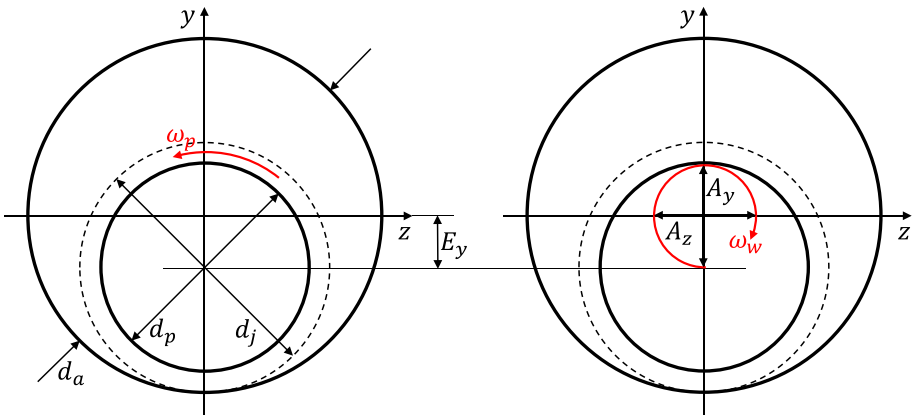

Fig. 2. Geometrical and kinematical system quantities, downstream orientation. Left: Geometrical dimensions of drill pipe, tool joints and outer wall of wellbore as well as drill pipe rotation around its own axis. Right: Kinematic quantities describing whirling motion of drill pipe in wellbore.

Table 1
Coefficients for second-order polynomials c1+c2rpmp + c3Qf + c4rpmp2+c5rpmpQf + c6Qf2 describing Ey = f(rpmp, Qf) and Ay = f(rpmp, Qf) in the SP experiments of Khatibi et al. (2018a, 2018b). It is assumed that for rpmp = 0 and Qf > 0 the datapoints show the same trend as for rpmp = 0 and Qf = 0 (red marked in Table 6 in Appendix C).

Case	c1	c2	c3	c4	c5	c6
Ey	−0.007085	2.916e-06	0.04796	1.891e-08	0.003387	845.2
Ay	0.0003163	5.074e-05	−0.8467	−1.526e-07	−0.001904	560

Table 2
SP test matrix following the experiments of Khatibi et al. (2018a, 2018b). In case of non-zero drill pipe speed, whirling acc. to equations (1) and (2) as well as Table 1 was additionally specified.

Case	Fluid	Eccentricity	ω_p [RPM]
1	H_2O	0	0
2	H_2O	−0.95	0
3	H2O	−0.88	100
4	H2O	−0.77	200
5	H2O	−0.60	300
6	PAC	0	0
7	PAC	−0.95	0

Table 3
MP test matrix. In case of e_y = {SW, AW} a whirling motion acc. to equations (1) and (2) was additionally specified.

Case	Fluid	e_y [-]	ω_p [RPM]	dp/dx [Pa/m]
1	H_2O	−0.54	0, 30, 60, 100, 130	−100, −200, −300, −400, −500
2	H_2O	0.00		
3	H2O	0.54		
4	H2O	AW	30, 60, 100, 130	
5	H2O	SW		
6	PAC	−0.54	0, 30, 60, 100, 130	
7	PAC	0.00		
8	PAC	0.54		
9	PAC	AW	30, 60, 100, 130	
10	PAC	SW		

2.2. Test matrix

Table 2 summarizes the SP cases investigated for rotational and lateral-motion model validation.

For the cuttings transport multiphase (MP) simulations, a horizontal 8.5 in wellbore section ($d_o = 0.216$ m) with a 5.0 inch drill pipe ($d_p = 0.127$ m and tool joint diameter $d_j = 0.168$ m) was assumed. Different fluids, eccentricities/whirl types, pressure gradients and drill pipe rotation rates were investigated as summarized by Table 3 in order to represent field values.

For the sake of clarity, Fig. 3 details column e_y of Table 3, where the drill pipe's AW and SW motion is defined as described in section 2.1 and equations (1) and (2).

The properties of the two types of fluids investigated in this study are given in Table 4.

In all cases, following Khatibi et al. (2018a, 2018b), the solids were simplified as spherical particles with diameter $d_s = 1.2$ mm, density $\rho_s = 2650$ kg/m^3 and angle of internal friction $\alpha_{if} = 45°$. The solid loading was determined such that without flow and rotation, the solids bed was filling the lower clearance for the smaller eccentricity $e_y = -0.54$, which yields $\alpha_s = 0.047$.

2.3. Physical model

As a MP flow model, we here apply the TFM in combination with the KTGF developed by Savage (Lun et al., 1984; Savage et al., 1996; Savage and Jeffrey, 1981) handling the loose, i.e. the collisional/kinetic regime[3] (solid volume fraction $\alpha_s < \alpha_{s,f} = 0.55$) and closures from soil mechanics describing the dense regime ($\alpha_s > \alpha_{s,f}$) of the cuttings, hereafter termed solids. The two phases are considered as interpenetrating continua and mass continuity and momentum transport equations along with closures for the fluids and solids material functions, turbulence, and the momentum exchange terms are used to model the system. The full model description is given in 5 Appendix A.

As previous investigators (e.g. Epelle and Gerogiorgis, 2017; Pang et al., 2019, 2018; Zakerian et al., 2018), we utilize the model implementation of ANSYS Fluent (ANSYS, Inc., 2016a, 2016b), a broadly used commercial CFD code.

[3] In the literature, these regimes are alternatively known as the inertial or viscous regime and the plastic or frictional regime, respectively.

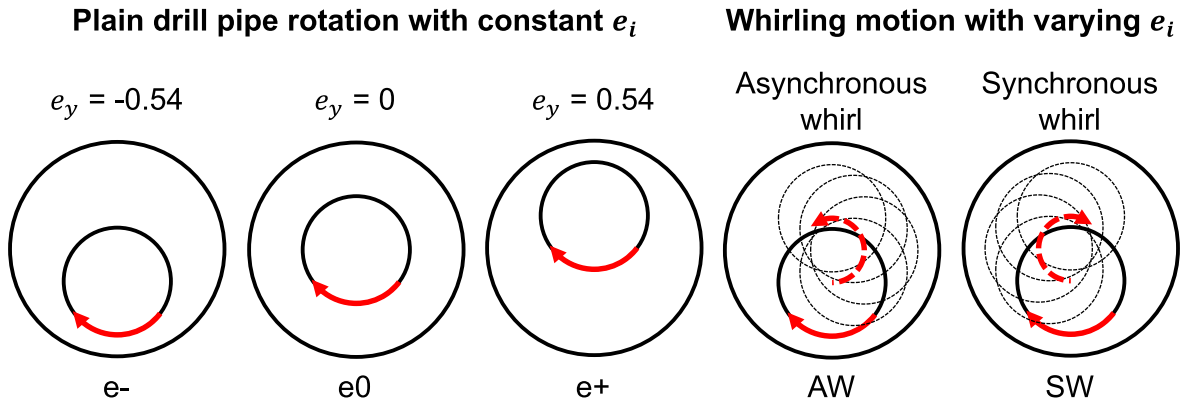

Fig. 3. *Overview of different systems investigated in terms of eccentricity e_i, plain drillpipe rotation around the drill pipe axis, and whirling motion of the drill pipe.*

Table 4
Fluid rheological model coefficients and density for different cases investigated based on the experiments of Khatibi et al. (2018a, 2018b).

Fluid	n_{PL} [-]	K_{PL} [Pa·s^n]	ρ_f [kg/m^3]
H_2O	1	0.001002	1000
PAC (PL)	0.86	0.025	

2.4. CFD setup & numerics

For the SP simulations, a variety of meshes of varying eccentricity based on Table 1 were created. Table 7 in Appendix E provides an overview of the relevant mesh parameters and Fig. 4 provides an eccentric example of the "Intermediate (MP)" case.

The dependency of the numerical solution on the mesh resolution was firstly evaluated with SP simulations (without rotation) as depicted in Fig. 19 in Appendix E. For all meshes, the r -spacing was non-uniform in order to obtain a higher resolution close to the walls. Periodic boundary conditions (BC), i.e., what leaves the domain enters the domain, were applied to either end of the annular element in order to reduce computational efforts. The length of the computational domain was chosen as $L = d_o$ for the SP, and $L = 3d_o$ for the MP simulations (such that any periodicity in the solution is not influenced by the BC).[4] The "Coarse (High Re)" mesh and the "Superfine (Low Re)" mesh results differ by only 1%, while the "Intermediate" mesh result differs from the "Superfine (Low Re)" mesh result by 3.8%. However, the "Intermediate" mesh does feature a much smaller first layer more suited for larger flows/pressure gradients (and thus steeper wall gradients) and it represents the experimental data best. Fig. 20 in Appendix E shows transient results for a MP case for the "Intermediate (MP)" and "Fine" meshes. In the near-steady-state time period, the difference between the two meshes is <1% for U_f and about 5% for U_s. The selected mesh quality "Intermediate" provided a fair compromise between sufficiently accurate results in the form of time-averaged integral quantities (Goldschmidt et al., 2004) such as superficial velocities/mass flow rates and associated computational effort and is comparable to similarly sized grids in other studies (e.g. Epelle and Gerogiorgis, 2017; Rooki et al., 2013b, 2013a; Zakerian et al., 2018).

The plain rotation of the drill pipe around its own axis was defined as a slip velocity of the inner wall, i.e., the fluid velocity at the wall is not zero but has a magnitude and direction equivalent to the wall rotational speed of the drill pipe. In case of SP simulations, we specified a mass flow rate, while in case of MP simulations a mixture pressure gradient $\Delta p/\Delta x$ along with the solid volume fraction α_s was specified.Fluent's dynamic meshing capability was employed to deform the mesh and simulate the orbital motion of the inner pipe. The latter was defined by an User-Defined-Function (UDF) which is simply an implementation of the time derivative of equations (1) and (2) and provides the velocities of the center of gravity of the orbital motion of the drill pipe to the solver. The spring-based smoothing method, were the cell edges are treated as elastic springs, was used to update the mesh every time step.

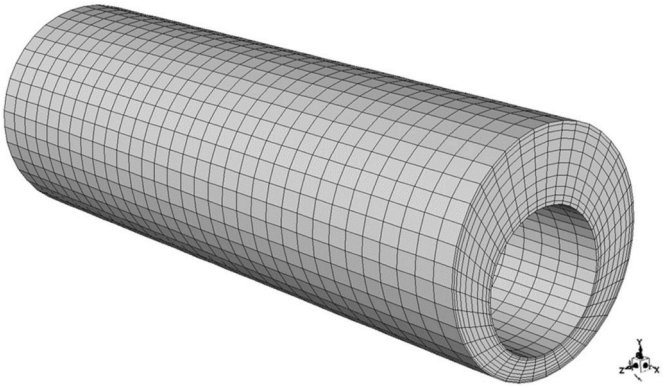

Fig. 4. Initial grid for negative eccentric and whirling motion cases. Full video showing trajectory of drill string whirling motion available at https://youtu.be/vV-0C9GXkWM.

All simulations but the SP mesh dependence cases depicted in Fig. 19 in Appendix E were performed in a transient manner, as exemplarily depicted in Fig. 20 in Appendix E. The time step was 10^{-3} s to 10^{-4} s and a second-order implicit scheme was employed. The (Phase-Coupled) SIMPLE scheme (Vasquez, 2000) was used for pressure-velocity coupling. The QUICK scheme (Leonard, 1979) was used for second-order spatial discretization and the Green-Gauss node-based gradient scheme was used to evaluate all gradients. The time discretization was implicit second order. The algebraic multigrid method with the Gauss-Seidel solver and conservative under-relaxation factor settings were used to solve the system of discretized equation.

At t = 0 the solids were patched into the domain and then allowed to settle over time until a partly moving-partly stationary bed is built up, resulting in an quasi-steady state of U_f and U_s, as illustrated by Fig. 20. Simulations were then continued for at least five orbital motions for the purpose of data sampling.

Pre-studies showed that the mesh deformation works fine for a couple of orbital motions only. After six to twelve orbital cycles, the

[4] Even though a RANS framework is adopted, we did not know whether the drill string dynamics would generate any irregular solid particle motions in the streamwise direction. Therefore, we decided to employ a domain where, for the given dimensions, the length is about 14.5 times the mean gap. This is about 4.3 times the largest gap occurring in the eccentric cases studied. However, no streamwise dependency of any flow quantities where observed.

mesh starts to deform non-uniformly and eventually highly skewed cells lead to negative volume and divergence. We therefore simply replaced the mesh after a preset number of orbital cycles (two to four) with the initial, where the solver transfers the current solution from the old to the new mesh using interpolation schemes. Reducing the time step size did not rectify the mesh deterioration.

3. Results

We first present results which to some extent validate the CFD model with available experimental data. Secondly, we present results for the industrially relevant 8.5 inch wellbore section flow case where we focus on the effect of whirling motion on cuttings transport and the transitional flow regime.

3.1. Validation with single-phase experimental data

For validating the CFD model we hereafter present SP results benchmarked with respective experimental data and friction factor correlations. We use the experimental data of Khatibi et al. (2018a, 2018b) because besides containing data for transitional flow of PL fluids, this data set also contains data for whirling drill string motion. In their experiments, Khatibi et al. (2018a, 2018b) used water and a shear-thinning 1 g/L polyanionic cellulose solution (PAC). A broad variety of friction factor correlations for turbulent concentric and eccentric annular flow is available in the literature. For instance, for the fully eccentric annular turbulent flow of different concentrations of drag-reducing guar gum solutions, explicit friction factor correlations as a function of the generalized Reynolds number, diameter ratio, and relative roughness are available (Dosunmu and Shah, 2015; Ogugbue and Shah, 2011). Other examples are the works of Kelessidis et al. (2011) and Pilehvari and Serth (2009) for the flow of bentonite suspensions. However, to our knowledge, no dedicated friction factor correlation for PAC solutions exists. For the case of PAC, we therefore utilize the correlations of Dodge and Metzner (1959) and Irvine (1988), which are corrected for eccentricity (Haciislamoglu and Cartalos, 1994; Haciislamoglu and Langlinais, 1990), if required.

Fig. 5shows CFD results for the flow of water in a concentric and fully eccentric annulus without pipe rotation.

The results are benchmarked with the aforementioned friction factor correlations from the literature. In addition, experimental data (Khatibi et al., 2018a, 2018b) is depicted. The reason for choosing this particular experimental data set is that it also contains data for whirling drill string motion.

While the CFD predictions adequately fit the empirical relations for both the concentric and eccentric annular configurations, the experimental data for the eccentric case falls slightly on top of the concentric flow data.

A zoom on the low superficial velocity range of Fig. 5 (black box) is depicted in Fig. 6.

In addition, CFD results for three different whirling motion cases are depicted along with the corresponding experimental results (Khatibi et al., 2018b). Note that the maximum eccentricity and the predefined whirling motion parameters for these cases are functions of the drill pipe rotational speed and the superficial fluid velocity and only valid for the experimental setup of Khatibi et al. (2018a, 2018b). With increasing rotational speed and the corresponding change of whirling motion, the respective pressure gradient increases. Interestingly, the aforementioned difference between CFD and experimental results is not observed for the 100 and 200 rpm cases. However, the 300 rpm cases are heavily underpredicted by the CFD simulations.

Finally, Fig. 7 provides pressure gradient vs. superficial fluid velocity results for the flow of PAC, both for the concentric and the eccentric case.

While there is good agreement between the friction factor correlations, CFD results and, in the eccentric case, the experimental data in the lower (laminar) range of superficial fluid velocities, this is not so for the higher (transitional) range. Compared to the friction factor correlations, the CFD results overpredict the transitional regime by up to 40%. In case of the eccentric configuration, CFD and experimental results show good agreement up to $U_{f,x} = 1.4$ m/s, where the experimental results start to deviate from the CFD results and approach the friction factor correation at higher $U_{f,x}$.

3.2. Validation with multi-phase experimental data

Concerning MP flows, the physical model as presented in Appendix A and its implementation in Fluent as used in this study has been validated to a good extent by several other researchers as depicted in Fig. 8 for the case of non-whirling flow cases and based on the non-dimensional Π-space of Busch et al. (2019). Except for the Cuttings Transport Ratio (CTR) and, to some extent, the Taylor number *Ta*, our parameter space as given by Tables 3 and 4 is encompassed in the spaces of previous studies. The lower CTR is a consequence of our comparatively high fluid superficial velocities. Most previous studies have validated their models with cases where the drill pipe is not rotating ($\rightarrow Ta = 0$), the reason is—from our point of view—that in many experimental studies the drill pipe is actually allowed to move freely but unfortunately this is often not clearly communicated. Therefore, high-quality experimental data suited for validation purposes is scarce.

3.3. Cuttings transport studies

While there are many ways to quantify the efficiency of cuttings transport and hole cleaning (A. Busch et al., 2018a), we here apply the *CTR* as the ratio of the two superficial phasic velocities (Bourgoyne et al., 1991, p. 178), i.e.

$$CTR = \frac{U_s^s}{U_f^s}, \tag{3}$$

where the superficial velocities are defined as

$$U_i^s = \frac{1}{A}\int_A \left(\alpha_i(y,z) \quad u_i(y,z) \right) dA, \quad i \in \{f,s\}, \tag{4}$$

where u_i are the respective phasic x -velocity components and A is the cross-sectional area.[5]

This *CTR* choice is mainly motivated by the specification of the mixture pressure gradient $\Delta p/\Delta x$ and the solid volume fraction α_s as input parameters in our numerical simulations due to the periodicity of our computational domain. Hence, the latter constitutes a fixed mass of solids and hence predetermined bed height in the absence of flow. Therefore, the superficial velocities and the pressure gradient constitute the response of the system. For clarity, it is important to realize that the results presented do compare to each other in terms of dp/dx equivalence only and not in terms of equivalence of U_f^s (or U_s^s). While the latter is often used in the literature and is beneficial because the flow rate is known a priori, from a controls engineering point of view the former is sounder: While the volumetric fluid flow rate may be the primary variable to manipulate during operations, it is the pressure gradient which is monitored and to be kept below critical values.

For the different cases defined and depicted in Table 3 and Fig. 3, respectively, and H2O as the fluid phase, Fig. 9 shows the *CTR* plotted vs. drill pipe rotation and dp/dx.

In the absence of whirling motion, the *CTR* is highest for the positive eccentricity and lowest for the negative eccentricity. The effect of plain

[5] Note that as the phases are incompressible the definition of the superficial velocities provided in equation is equivalent to the volumetric flow rates, i.e. Ui = Qi = ρimi.

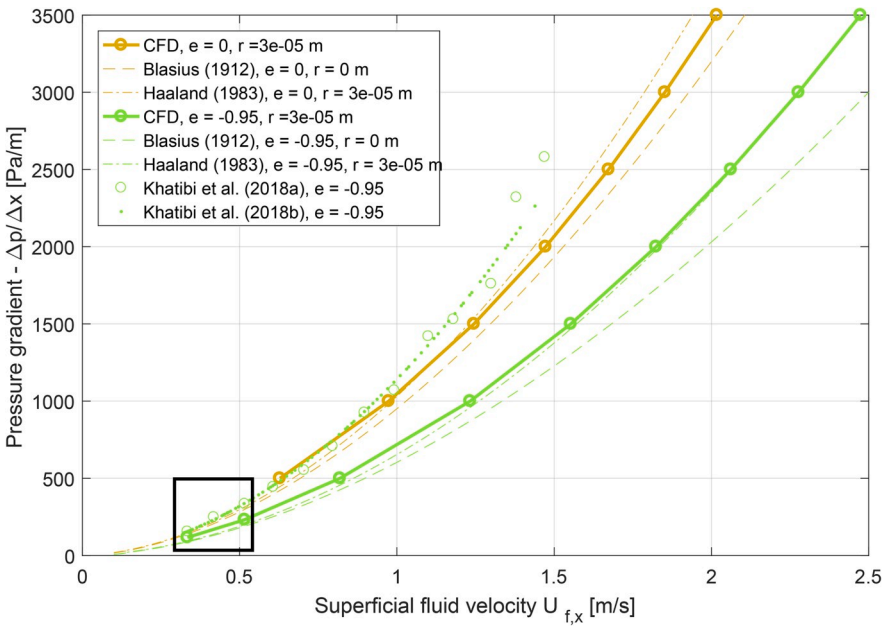

Fig. 5. CFD (solid lines) and experimental (marker symbols) pressure gradient $\Delta p/\Delta x$ vs. bulk velocity $U_{f,x}$ comparison for the e = −0.95, 0 rpm H_2O case of Khatibi et al. (2018a, 2018b). In addition, CFD results for a concentric annulus are depicted. Empirical correlations for both the concentric and eccentric—corrected for eccentricity (Haciislamoglu and Cartalos, 1994; Haciislamoglu and Langlinais, 1990)—case are plotted with dashed lines. The black box highlights the area depicted in Fig. 6.

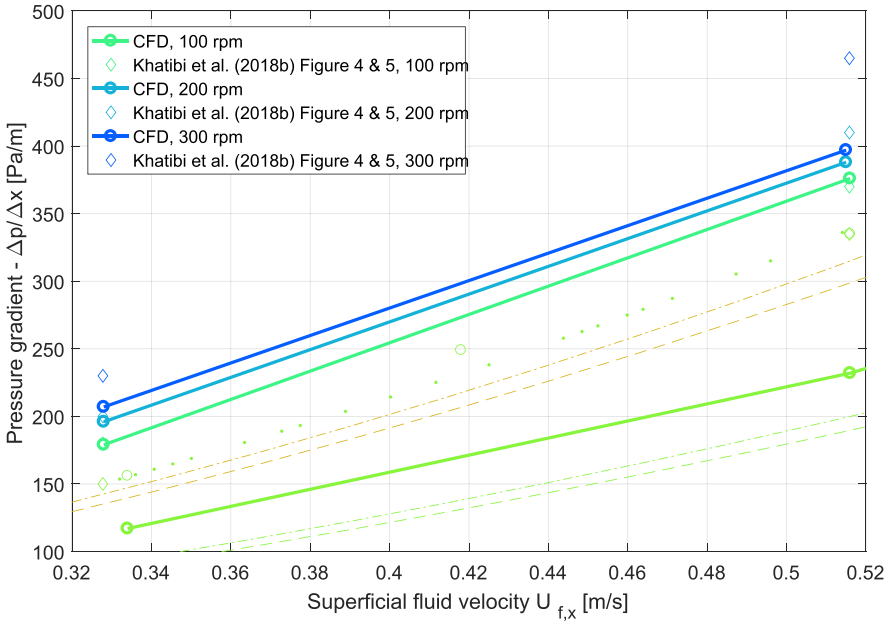

Fig. 6. CFD and experimental (time-averaged) data (Khatibi et al., 2018b) for various rpm cases. With regards to the non-rotating cases depicted in Figs. 5 and 6 depicts a zoom on the low $U_{f,x}$ -region of Fig. 5. For the respective legend information see Fig. 5.

drill pipe rotation is generally highest in the case of negative eccentricity. However, for higher pressure gradients, it similarly increases the *CTR* for the positive eccentricity case.

The presence of whirling motion significantly increases the *CTR* for rotational rates faster than 60 … 100 rpm. AW leads to *CTR* levels between concentric and positive eccentric drill pipe arrangements, while SW is outperforming all other cases for rotational rates faster than 60 … 100 rpm.

For the different cases depicted in Fig. 3 and PAC as the fluid phase, Fig. 10 shows the *CTR* plotted vs. drill pipe rotation and dp/dx.

As in the Newtonian case, the CTR is highest for SW, given that rotational rates larger than 60 … 100 rpm are maintained. As opposed to the Newtonian case, the AW case falls between the negative and concentric cases for the entire range of rotational rates.

The effect of plain drill pipe rotation is largest for the negative eccentric case and virtually non-existent for the positive eccentricity. For the concentric case, the *CTR* jumps from one level to another between 30 and 60 rpm.

In addition to the $CTR = f(rpm, dp/dx)$, we provide the results in the form $ROP = f(rpm, dp/dx)$, where *ROP* is related to the superficial solid velocity as the nominator of the *CTR* as follows: In a real field scenario at steady-state (with respect to all input parameters such as U_f^s and *ROP*), the superficial velocity of the solids U_s^s is determined by the *ROP*, the bit diameter D_o, and the rock porosity α_r as a consequence of mass conservation.

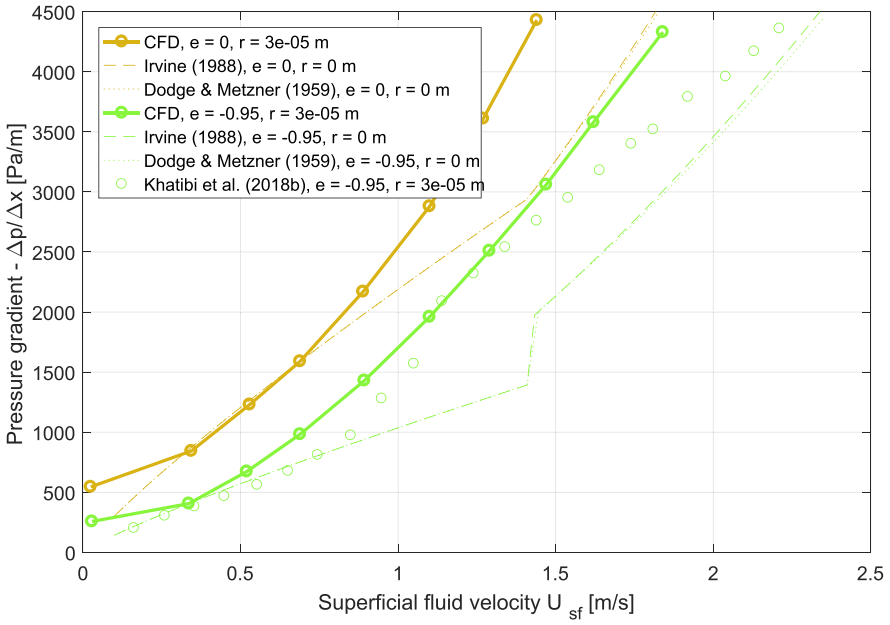

Fig. 7. CFD (solid lines) and experimental (marker symbols) pressure gradient $\Delta p/\Delta x$ vs. bulk velocity $U_{f,x}$ comparison for the e = −0.95, 0 rpm PAC case (Khatibi et al., 2018a). In addition, CFD results for a concentric annulus are depicted. Empirical PL correlations for both the concentric and eccentric—corrected for eccentricity (Haciislamoglu and Cartalos, 1994; Haciislamoglu and Langlinais, 1990)—case are plotted with dashed/dotted lines.

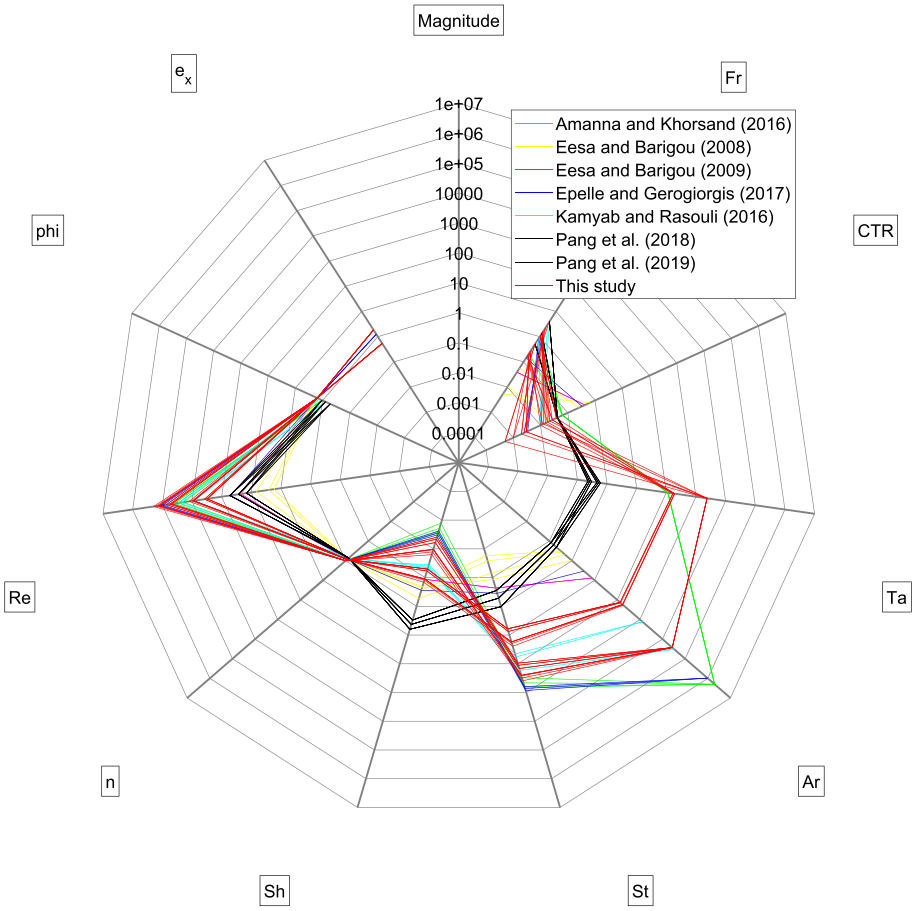

Fig. 8. Validation works of the physical model as summarized in 5 Appendix A and its implementation in ANSYS Fluent vs. this study based on the Π -space of the non-whirling flow case (Busch et al., 2019).

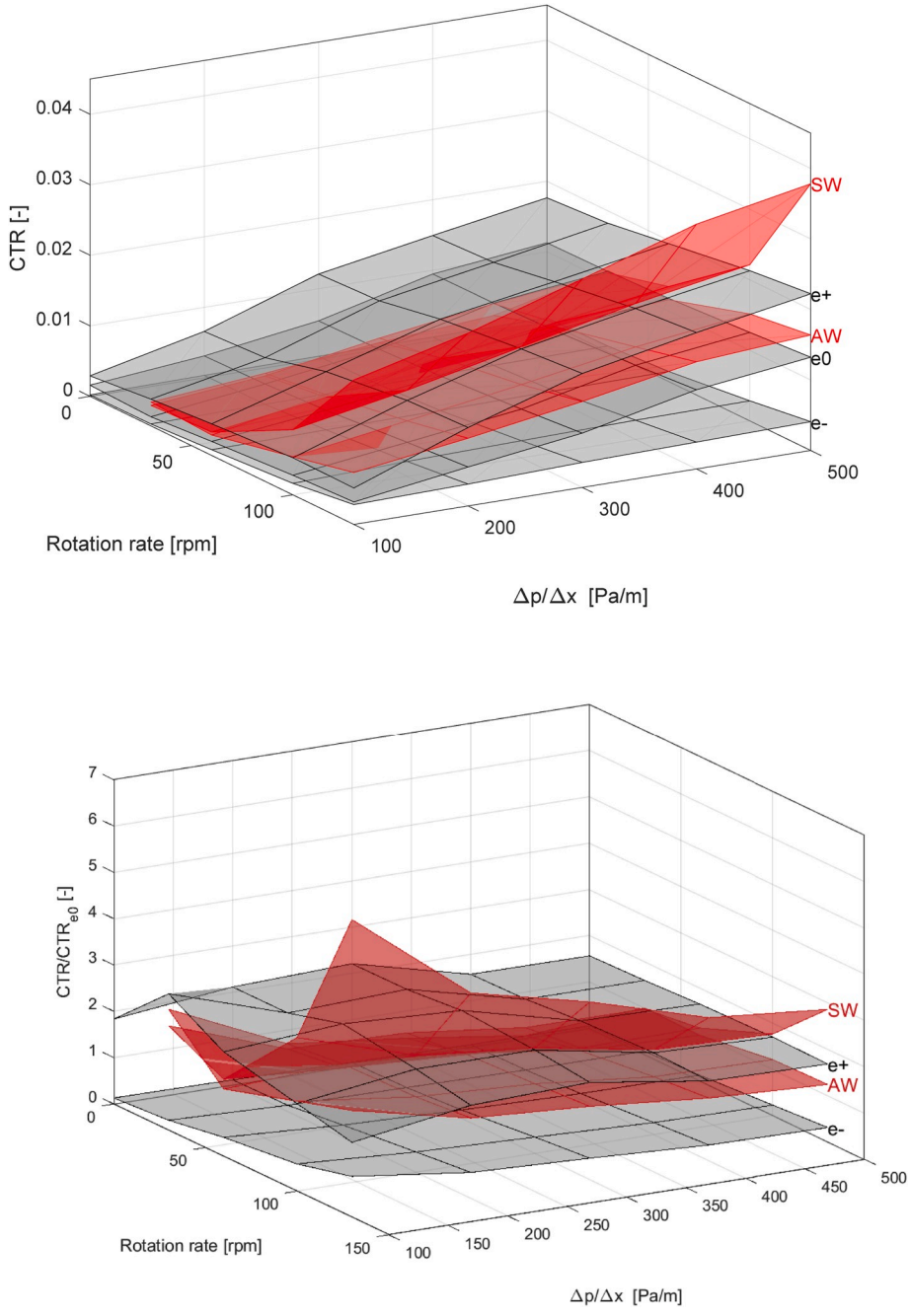

Fig. 9. Top: Absolute CTR vs. drill pipe rotation rate and pressure gradient for H2O and the systems defined in Fig. 3. Bottom: Relative change of the CTR based on the concentric system e0.

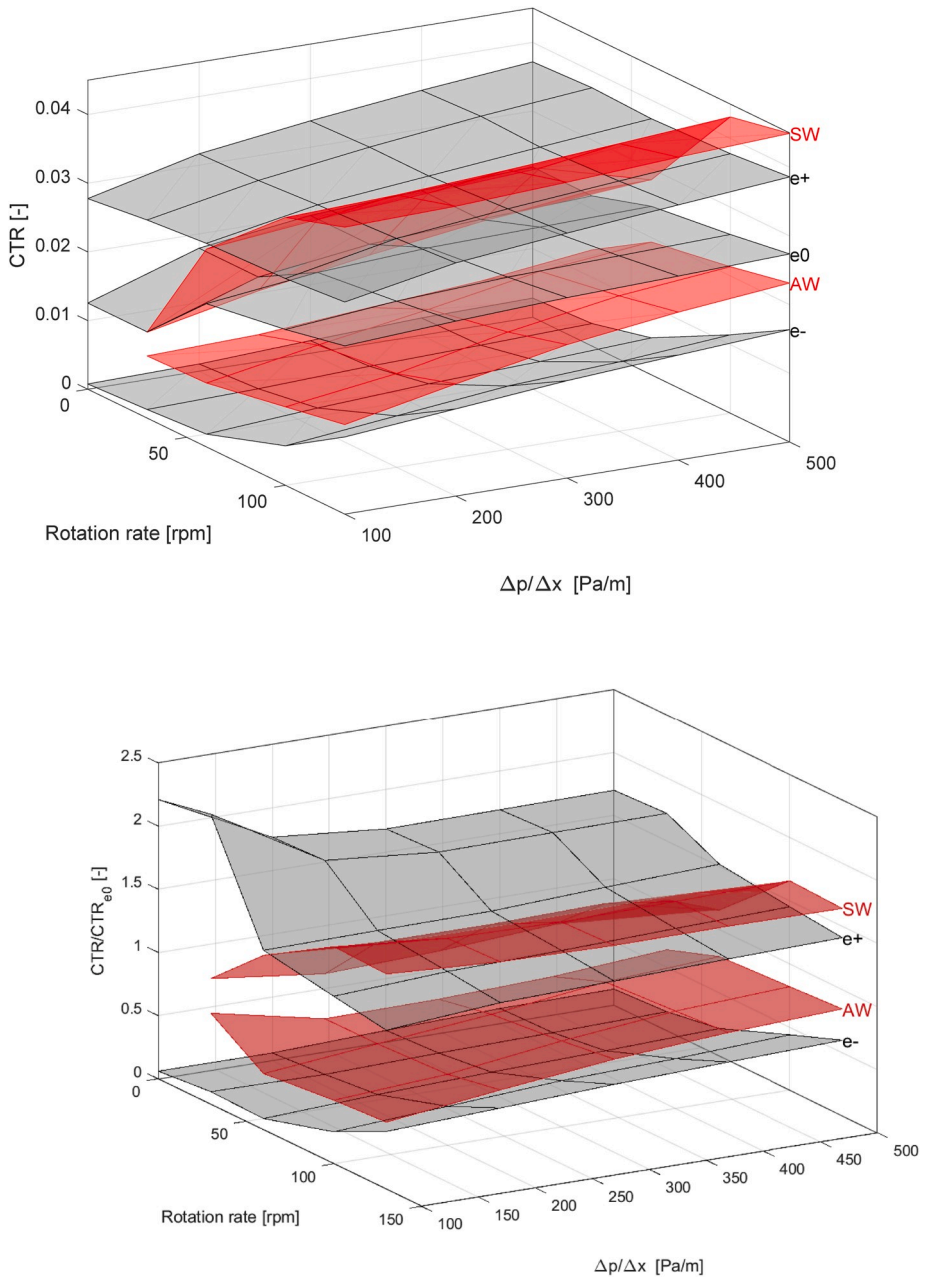

Fig. 10. Top: Absolute CTR vs. drill pipe rotation rate and pressure gradient for PAC and the systems defined in Fig. 3. Bottom: Relative change of the CTR based on the concentric system e0.

$$\frac{\pi D_o^2}{4} ROP(1-\alpha_r) = \frac{\pi\left(D_o^2 - D_i^2\right)}{4} U_s^s \tag{5}$$

While we find the same qualitative results for the case of H2O (Fig. 11), this is not so for the case of PAC (Fig. 12), where in contrast to the $CTR = f(rpm, dp/dx)$ presentation of Fig. 10 the positive eccentricity yields the highest *ROP* for the entire range of rotational rates considered and hence performs best in terms of hole cleaning.

To further illustrate the effect of the varied parameters on the results, we additionally depict the fluid superficial velocities for H2O and PAC in Fig. 13 and Fig. 14, respectively.

As expected, due to the different viscosity magnitudes, the fluid throughputs of PAC consistently fall under the levels of H2O for a given dp/dx.

For the concentric and positive eccentric cases, the effect of rotation is a bit more pronounced at lower dp/dx, and correspondingly fluid superficial velocities. For the negative eccentric case, as opposed to the H2O, a plateau exists for rotation rates >100 rpm in case of the PAC solution.

For any given pressure gradient, orbital motion results in a significantly reduced throughput for the entire range of rotational rates considered.

4. Discussion

4.1. Validation with single-phase experimental data

For the SP H2O base case (Re = 4900, $e = -0.95$, 0 rpm) of Khatibi et al. (2018a), the CFD results do fairly well fit the empirical pressure drop correlation (Blasius, 1912; Haaland, 1983) with the eccentricity correction (Haciislamoglu and Cartalos, 1994) applied. However, the experimental results (Khatibi et al., 2018a) exceed the CFD results by

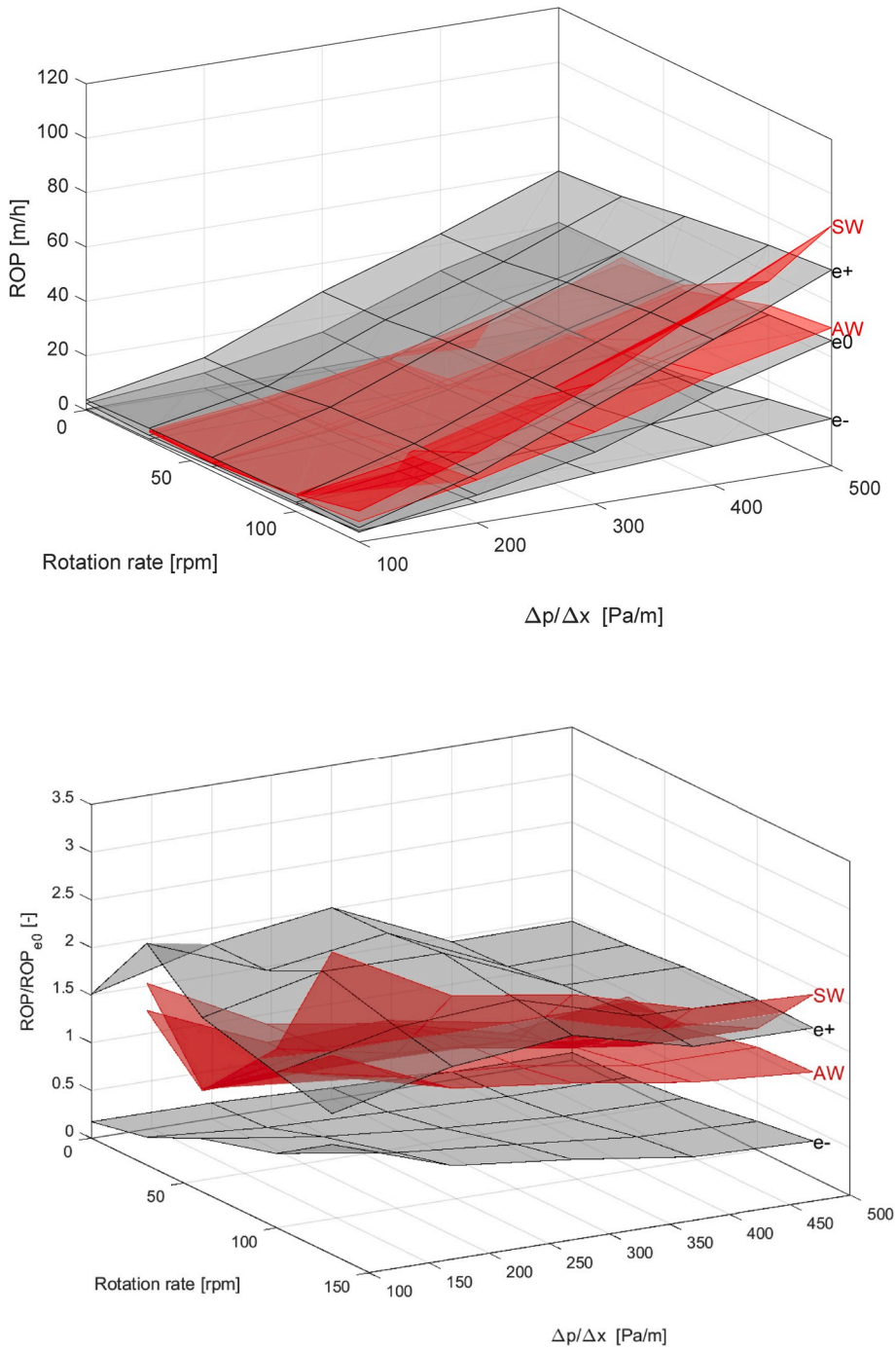

Fig. 11. Top: Absolute ROP vs. drill pipe rotation rate and pressure gradient for H2O and the systems defined in Fig. 3. Bottom: Relative change of the ROP based on the concentric system e0.

50% and do coincide with the fully concentric CFD results, which also match well with the empirical correlation (Blasius, 1912; Haaland, 1983). The significantly larger pressure drops found in the experiments may be a result of different factors. First, the computational domain assumes periodicity along x, which is not necessarily the case because of development length effects and a likely skewed whirling motion of the drill string.

The predefined whirling motion of the drill string is not necessarily describing the motion of the drill string for every x -location of the annulus. In the CFD model, we assume that the axis of the string and the outer pipe are parallel. However, due to the compliance of the drill pipe material as well as the flexible joints and the concentric fixation of the drill string at the motor end it is very likely that the drill string in the experiments features more complex whirling motion, which additionally varies in the streamwise direction, i.e. is skewed along x. Closer to the motor end it will naturally feature a more concentric and less whirling motion while further away of the motor it may move more freely and hence feature more complex elliptic motion patterns as indicated in Fig. 1 of Khatibi et al. (2018a). This is corroborated by the geometrical constraints introduced by the flexible drill string section joints with an outer diameter $d_j = 0.031$ m (Khatibi, 2018) which yields a dimensionless eccentricity $e = -0.6$, whereas the factual eccentricity for the no flow/no rotation situation as reported by Khatibi et al. (2018b) was $e = -0.94$ (see tabulated data in Table 6/Appendix C). In addition, the

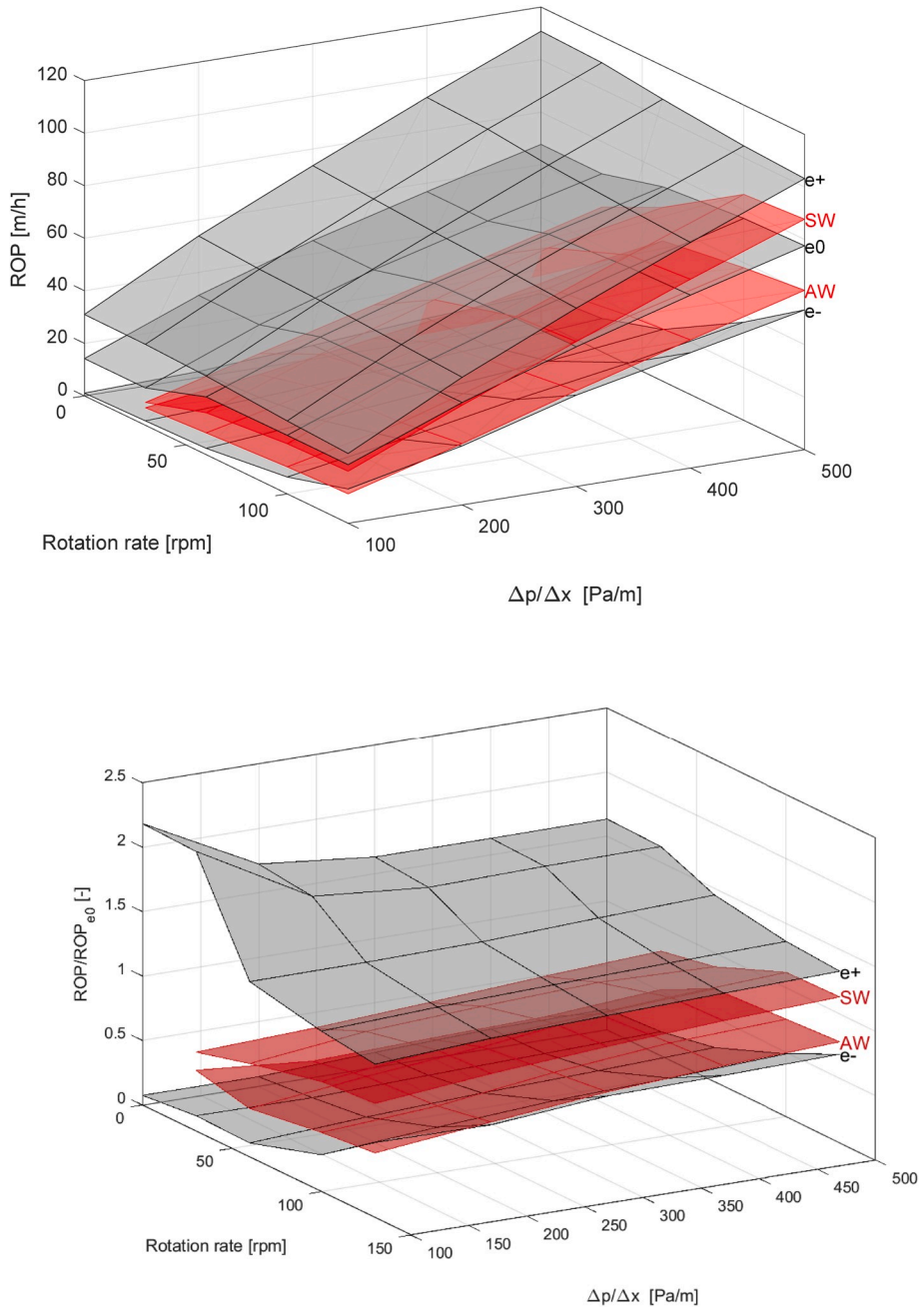

Fig. 12. Top: Absolute ROP vs. drill pipe rotation rate and pressure gradient for PAC and the systems defined in Fig. 3. Bottom: Relative change of the ROP based on the concentric system e0.

parameters characterizing the whirling motion of the drill pipe, namely the y - and z -amplitude and the frequency, were not precisely measured but rather estimated based on the obtained experimental data. The data characterizing the vertical eccentricity and amplitude of the drill string does not cover the entire parameter space and was obtained by graphical analysis of the PIV pictures. Both the horizontal amplitude and the frequency of the whirling motion where simply estimated based on visual observations rather than directly measured.

Furthermore, hydrodynamic entrance effects may be of relevance. For the laminar flow of water in a concentric annulus with $d_i/\ d_o > 0.5$, the development length may be estimated with $x_d = d_h/2(1-0.119\ln(d_i/d_o))(0.631^{1.6} + (0.0442\mathrm{Re})^{1.6})^{1/1.6}$ (Poole, 2010), which gives 1.71 m for the Re = 4900 case and 2.69 m for the Re = 7700 case. In contrast, in case of turbulent flow, the development length is much shorter and may be estimated with $4.4 d_h \mathrm{Re}^{1/6}$ (Çengel and Cimbala, 2006), which yields only 0.27 m and 0.29 m, respectively. However, Lien et al. (2004) recommend $150 d_h/2$, which yields 1.25 m.

In any case, here we are dealing with transitional flow, which is intermittent in the sense that both laminarization and development of turbulence are competing. In the experiments of Khatibi et al. (2018a, 2018b), the distance from the beginning of the annular section to the first pressure transducer is 1.4 m, and 1.52 m from the first to the second pressure transducer. Moreover, 0.3 m prior to the first pressure transducer, the first flexible joint with an outer diameter $d_j = 0.031$ m (Khatibi, 2018) significantly reduces the cross-sectional flow area and hence introduces a flow disturbance. Thus, the flow may still have been of developing nature in the section where pressure measurements were taken.

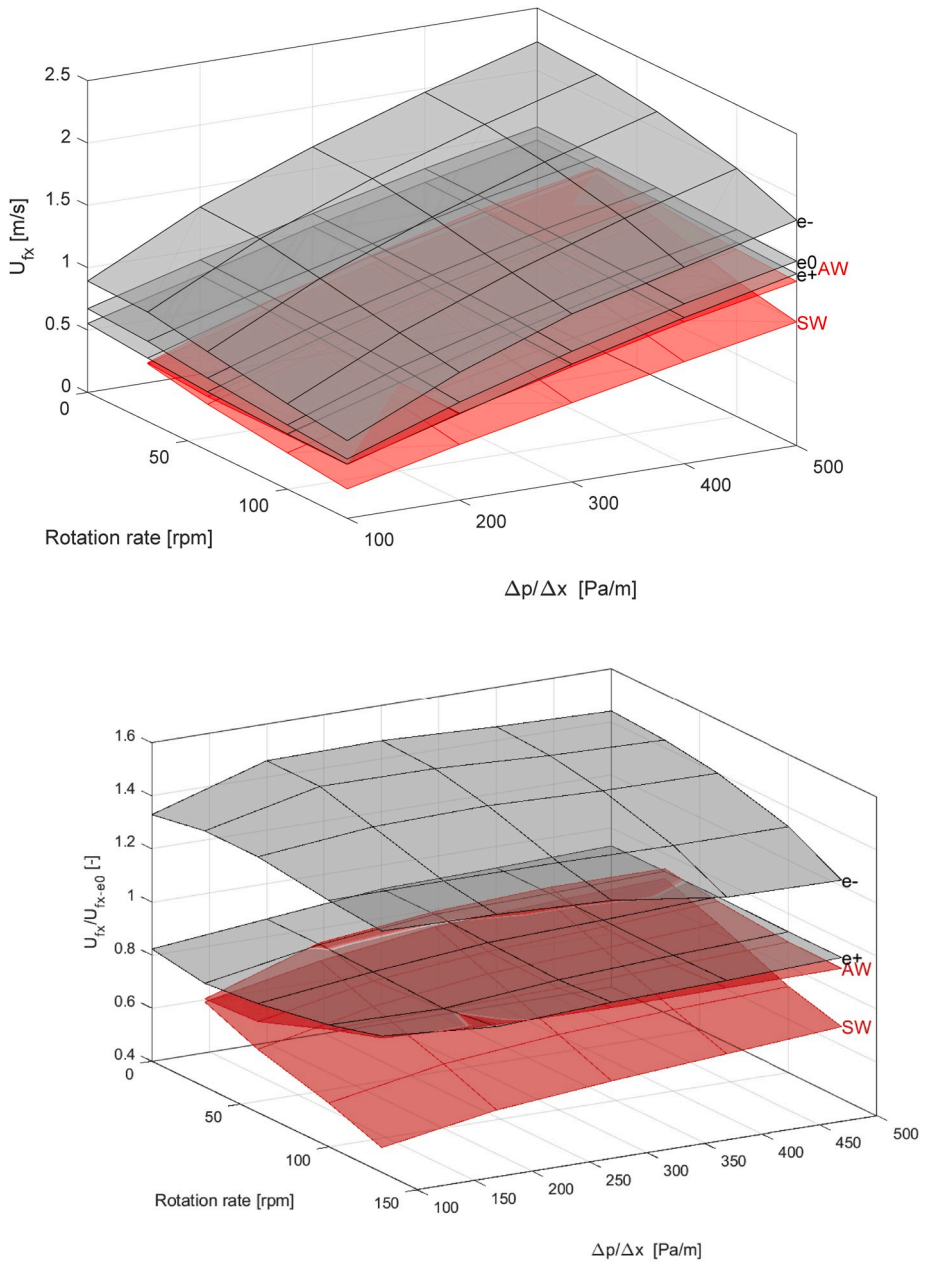

Fig. 13. Top: Absolute fluid superficial velocity vs. drill pipe rotation rate and pressure gradient for H2O and the systems defined in Fig. 3. Bottom: Relative change of the fluid superficial velocity based on the concentric system e0.

Finally, in the case of PAC, the discrepancies between CFD and experimental results as well as the friction factor correlations may be attributed to the viscoelastic and/or drag-reducing capabilities of the PAC solutions utilized (Alexander Busch et al., 2018b). The Generalized Newtonian Fluid framework with the PL material function does neither account for normal stress differences nor for elongational viscosity, both of which affect flows in eccentric annuli with the latter also affecting rotational flows (Escudier et al., 2002). Moreover, while the employed k-ω SST model is versatile regarding $y+$ values it does neither consider n_{PL} -dependent damping functions (e.g. Malin, 1997) nor non-Newtonian wall functions (e.g. Johansen and Mo, 2015) in the $y+ < 1$ and $y+ > 30$ regimes, respectively.

4.2. Cuttings transport – plain drill pipe rotation

Focusing on the plain drill pipe rotation cases first, the positive eccentric case generally leads to much better hole cleaning than the eccentric case, in line with other studies (Bicalho et al., 2016a; Heydari et al., 2017). The more clearance between the drill pipe and the cuttings bed, the better the hole cleaning because of the higher fluid velocities below the drill pipe and on top of the sediment bed. Consequently, the shear stress acting on the bed is much higher for a positive eccentric drill pipe than for a negative eccentric one, hence the better *CTR* and *ROP* values. This is physically sound and in accordance with the often-stated order when it comes to the relevance of individual cuttings transport parameters: Volumetric fluid flow rate is typically considered the most important parameter, simply because it is just the axial flow components which transports solids. Drill pipe rotation is an additional contributing factor which depends on the flow regime, fluid rheological parameters, and, as shown, eccentricity. It is important to note that the results were obtained for a total solid volume fraction $\alpha_s = 0.047$. Larger values will lead to a higher cuttings bed in the computational domain, which will

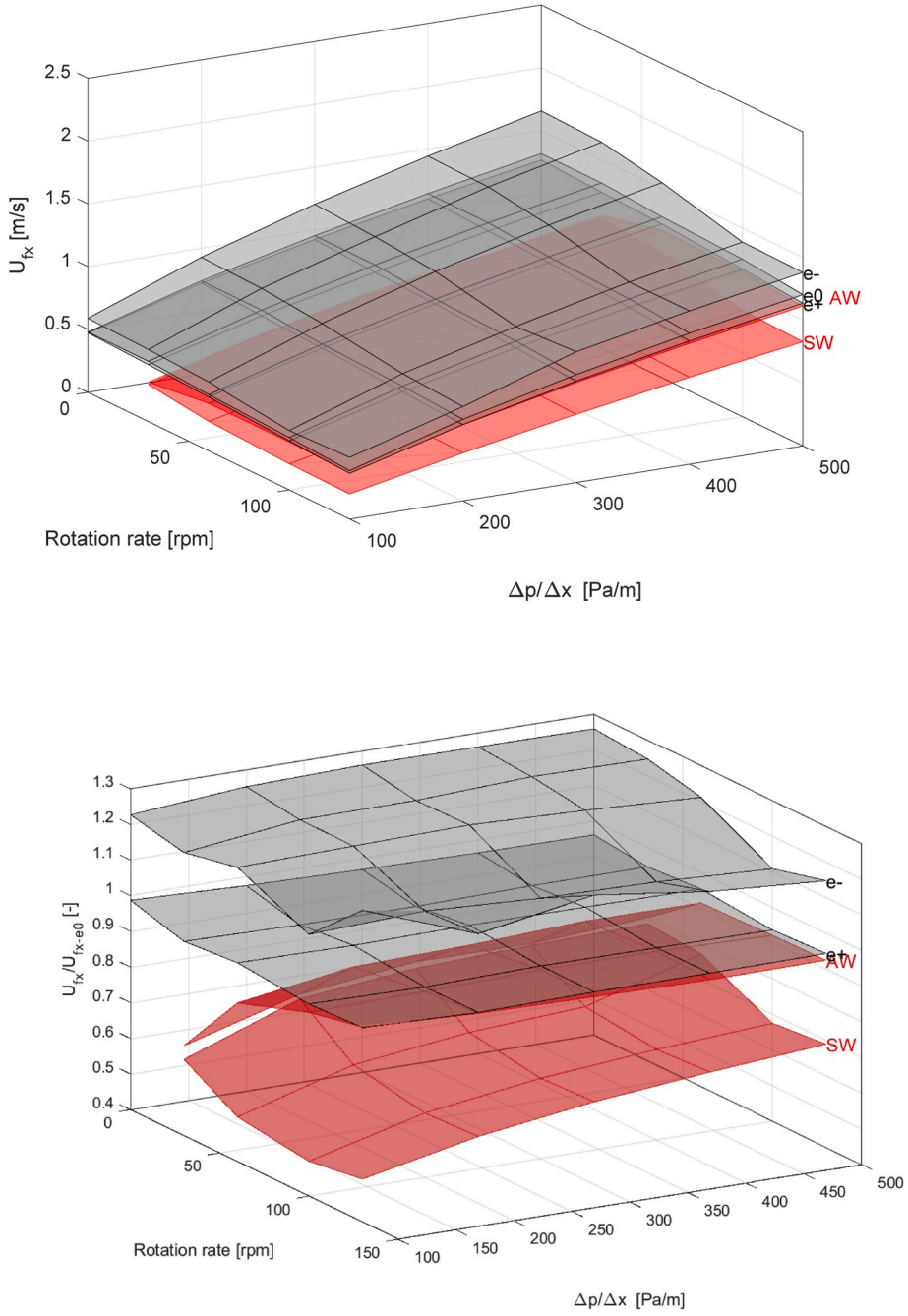

Fig. 14. Top: Absolute fluid superficial velocity vs. drill pipe rotation rate and pressure gradient for PAC and the systems defined in Fig. 3. Bottom: Relative change of the fluid superficial velocity based on the concentric system e0.

change the picture.

The effect of plain drill pipe rotation is highest for the negative eccentricity because the corresponding tangential velocities of the fluid and subsequently the solid phase act directly on the bed, agitate the bed and disperse solids into regions of higher fluid velocity, where they are easily transported downstream. This effect is less prominent in the other configurations. However, it is also less relevant for hole cleaning in the other configurations because of the aforementioned role of the locally higher fluid streamwise velocities and the higher shear stresses acting on the bed.

For a shear-thinning fluid in laminar flow, rotation may generally reduce the pressure gradient, i.e. increase the throughput for a given dp/dx. In contrast, in turbulent flow, rotation may increase the pressure gradient, i.e. decrease the throughput for a given dp/dx, as it increases the degree of turbulence. For the investigated shear-thinning PAC solution, this effect is very small, presumably because shear-thinning and turbulence generation are counteracting each other as the flow is in fact transitional rather than fully turbulent (see Fig. 18 in Appendix D). In addition, the presence of solids certainly overshadows this SP effect.

4.3. Cuttings transport – whirling motion

Assuming a concentric drill pipe as the base case, the presence of whirling motion generally increases both the *CTR* and the *ROP*. The same mechanism as for plain drill pipe rotation applies: The additional whirling motion leads to an increase in tangential and here additionally radial (with respect to the streamwise flow direction) velocities which help to agitate the sediment bed and disperse cuttings into the main flow regions and thus enhance cuttings transport. Note that in case of the shear-thinning PAC, the SW and AS *ROP* is less than for the concentric case and only for higher $\Delta p/\Delta x$ SW outperforms the concentric arrangement. The orbital drill pipe motion leads to two counteracting effects: (1) A reduction of the viscosity due to the additional applied shear and (2) the agitation of the bed due to the increase of turbulence and increased tangential/radial velocities, the.second one becoming dominant for higher $\Delta p/\Delta x$.

The SW significantly outperforms the AW because in case of SW both the tangential velocity induced by the drill pipe motion around its own axis and the radial velocity induced by the drill pipe orbital motion act in the same direction and are therefore additive. In case of AW, the plain drill pipe rotation is in the opposite direction of the drill pipe orbital motion and the respective velocities to some extent counteract each other.

In case of the PAC, the solids transport is highest for the positive eccentric case. For this geometrical arrangement, the rotation of the drill pipe around its own axis leads only to a minor shift of the cuttings bed towards the side of the annulus (Fig. 16 (top) in 5 Appendix A), with the majority of the helical flow pattern occurring on top of the main flow field. This is not so for the SW case (Fig. 16 (bottom) in 5 Appendix A), where the orbital motion of the drill pipe leads to a circumferentially alternating helical flow pattern affecting the entire volume of the annulus. While this is generally considered a positive feature in the sense of bed agitation, it also leads to a reduction in fluid throughput because much more fluid obeys the induced helical motion (Fig. 14). This is also the case for H2O SW (Fig. 13), where the difference lies in the magnitude of velocities and viscosities associated with the two fluids. In case of H2O SW, the circumferentially alternating helical flow pattern leads to much less tangential flow (Fig. 15 in 5 Appendix A) and hence allows for more throughput. This indicates that (synchronous) whirling motion is most effective in enhancing cuttings transport in presence of low viscosity fluids and larger rotation rates. However, more comprehensive data is required in order to adequately assess the coupled effect of whirling motion and fluid rheological properties.

An operational challenge currently discussed in the drilling industry is drilling with an *ROP* of 60 m/h and a drill pipe rotation rate of 60 rpm (Iversen and Islam, 2018). Figs. 11 and 12 suggest that this may be achieved by ensuring a positive eccentricity or SW state of the drill string in the wellbore in combination with a $dp/dx > 500$ Pa/m for H2O and $dp/dx > 250$ Pa/m for PAC. However, the quantitative results presented in Figs. 11 and 12 may not simply be applied to field scenarios because the modelling framework used is, for the multiphase part, neither validated nor tuned with experimental data.

4.4. Strength and weaknesses

The presented model and computational approach is a comparatively simple tool to analyze the effect of orbital drill pipe motion. As applied in this study, it allows for quantification of the effect of whirling motion on cuttings transport and qualitatively confirms the conclusion of Sanchez et al. (1999) that (if compared to an negative eccentric drill string arrangement) the orbital motion of the drill pipe is the major reason for significant improvement of cuttings transport.

While the model and code implementation as utilized in this study has been validated to a good extent by several other researchers (e.g. Amanna and Khorsand Movaghar, 2016; Epelle and Gerogiorgis, 2017; Kamyab and Rasouli, 2016; Pang et al., 2019, 2018) for the case of non-whirling flow cases (see Fig. 8), further validation work is required for the whirling cases. However, this requires experimental data where the kinematics of the orbital drill pipe motions are clearly quantified. i.e., a precise description of the drill string orbital motion is provided. If this is not so, any then required estimate of motion-relevant parameters likely leads to bad model predictions as the comparison of SP simulations and experimental results of Khatibi et al. (2018a, 2018b) has shown.

The design space must be analyzed more comprehensively. In terms of fluid rheological properties, more viscous fluids have to be investigated as well as the role of a potential yield stress in the presence of whirling motion. In addition, solid volume fractions, solid particle diameters, the pipe-hole-diameter combination and inclination, which is a critical parameter as it defines the potential for avalanches, is to be varied in order to obtain a broader quantitative picture of the relevance of whirling motion. Given enough data, one may then also transform the data easily into the more common $(\alpha_s, dp/dx) = f(U_f, \ldots)$ framework. More complex motion patterns need to be studied as we have just focused on easy-to-parametrize forward and backward whirl. Any slip between the drill pipe collars and the wellbore wall as well as detachment may occur in the wellbore. Furthermore, the presence of the cuttings bed will likely change the circular or elliptical orbital motion patterns typically utilized in the industry (due to their simple mathematical description). However, a bidirectional coupling of moving drill pipe structure and flow of fluid and solid phases is not reasonably possible on the annular scale as the structural deformation and associated non-flow forces depend on information up- and downstream of the annular domain under investigation.

While the applied GNF framework is the state-of-the-art in cuttings transport research, it does not account for potentially relevant physics such as thixotropy and viscoelasticity. Laboratory fluids such as CMC and PAC are known to act thixotropic and viscoelastic (Alexander Busch et al., 2018b), and the viscoelastic properties of drilling fluid systems as used in the field may lead to sediment bed cohesion (Werner, 2018) that is not captured by the GNF framework.

For higher superficial velocities, the model does not replicate pressure drop quantitatively well. Two effects come into play: (1) Too high values of the fluids viscosity are to be expected due to the utilized turbulence modelling approach, which will reduce particle settling and the mass flow rate for a given pressure gradient. As briefly mentioned in 5A.4, the RANS framework of commercial solvers in general and Fluent specifically does not account for the viscosity as a varying quantity. Generally, in RANS turbulence models, the rate of strain is defined as the symmetric part of the mean velocity field gradient. This neglects any additional variation due to the velocity fluctuations, which will lead to an underestimation of the rate of strain magnitude and thus

overestimation of the fluid viscosity. Note that the same holds for other two-equation models such as the often-utilized k -ε -model. (2) The high-Re approach taken is based on Newtonian wall functions which will likely produce incorrect estimates of the respective near-wall quantities in the non-Newtonian case.

The transport rate of solids through the domain may be overestimated by an unknown extent. The Eulerian-Eulerian method employed in this study, i.e. the Two Fluid Model (TFM) continuum approach with the Kinetic Theory of Granular Flow (KTGF) and additional closures to handle the dense granular regime, as implemented in Fluent R17.2, does not produce angle of repose satisfying conditions in the absence of flow under all conditions (Busch and Johansen, 2018). Even for a horizontal bed under the sole influence of gravity, the top-layer always remains in a liquid-like state regardless of flow time. The KTFG dynamics act in a checkerboard-like manner ensuring a very low viscous solid phase, which in the concept of the TFM continuum approach should feature high solid viscosity levels representing the non-flowing sediment bed. According to these observations, it is expected that the solids bed will behave as "fluidized" in the simulations and that the solids flux may be overestimated. An alternative and with respect to the above mentioned overestimation of the solids transport rate better-suited modelling approach is the CFD-DEM framework (e.g. Akhshik et al., 2015; Zhang et al., 2016), which if combined with the periodic BC approach as used in this study may also allow reasonable computation times.

Another issue with the TFM-KTGF-SM approach is the potential violation of its inherent continuum assumption for specific combinations of system sizes and particle sizes (Goldschmidt et al., 2004). For instance, the smallest mesh size as a consequence of the dynamic meshing technique employed is approx. 1.04 mm, which is in the order of the particle size d_p. This may lead to an error in regions of high fluid velocity or pressure gradients since interaction forces between phases will be simply computed based on the respective cell values. However, the same applies for Lagrangian methods. Alternatives, such as Fluent's Macroscopic Particle Model (Agrawal et al., 2004), are not fit for purpose due to the associated computational effort for the systems under consideration here.

The employed mesh moving feature of Fluent R17.2 led to severe mesh deformation with time. Depending on the orbital frequency, the mesh had to be replaced (i.e. the current solution is interpolated to a new mesh) after several seconds of flow time in order to avoid grid deterioration. The mesh motion feature of Fluent is not meant to be used for high rotational mesh deformation, therefore a sliding mesh approach as employed by Bicalho et al. (2016a, 2016b) may be the better choice.

The accuracy of the results may be increased by refining the mesh. This may be achieved at no additional computational costs by significantly shortening the domain since no streamwise development of any quantity was observed.

5. Conclusions & outlook

We have numerically investigated the role of whirling drill string motion on cuttings transport by means of CFD and a dynamic mesh technique. The essential findings are:

- In case of a negative eccentric annulus, whirling motion helps tremendously to disperse the solids into the main flow region and hence improves the quality of cuttings transport and hole cleaning. The effect is much more relevant for water than for the investigated more viscous, shear-thinning fluid because the latter already shows a good cuttings transport performance.
- Synchronous whirl is much better suited to agitate the bed and disperse cuttings than asynchronous whirl because the tangential and radial velocities add to each other.
- For the investigated parameter values, the positive eccentric annulus provides an even better cuttings transport capability for PAC being the carrier fluid. Whirling motion reduces the axial throughput, which despite the increased bed agitation results in worse performance compared to the positive eccentric case.
- The classical view of rotation being a relevant parameter for cuttings transports needs to be detailed: The cuttings transport research community needs to distinguish between plain drill pipe rotation around its own axis and rotation involving different types of whirling motion or more complex lateral motion patterns. Experimentalists are advised to carefully design their laboratory setups such that occurring whirling motion can be quantified.
- More research is required to explore the entire industry-relevant design space, i.e. other numerical values of the solid volume fraction, other fluids, inclination, and orbital motions. In addition, the laminar flow regime needs to be addressed. However, a bi-partisan approach is need where experimental work is conducted in order to validate and improve the simulation work.

CRediT authorship contribution statement

Alexander Busch: Conceptualization, Data curation, Formal analysis, Investigation, Methodology, Resources, Software, Validation, Visualization, Writing - original draft, Writing - review & editing. **Stein Tore Johansen:** Conceptualization, Formal analysis, Funding acquisition, Methodology, Project administration, Resources, Supervision, Writing - review & editing.

Acknowledgements

The project Advanced Wellbore transport Modeling (AdWell) with its sponsor, PETROMAKS 2/the Research Council of Norway (project 228391) and its partners Equinor, Neptune Energy Norge AS, NORCE, UiS, NTNU and SINTEF are gratefully acknowledged for funding and supporting this work. In addition, we are grateful for the computational resources provided at NTNU by UNINETT Sigma2 AS. Further, we thank the unknown reviewers for providing valuable input and improving the paper quality.

Appendix ASupplementary data

Supplementary data to this article can be found online at https://doi.org/10.1016/j.petrol.2020.107136.

Appendix A. Physical model

Appendix A1. The Cauchy equations of motion for a two-phase flow

In the TFM framework, the fluid (index f) as well as the solid (index s), phase are described as interpenetrating continua. Both fluid and solid are considered isothermal and incompressible.[6] For an arbitrary volume element V_i, the phase volume fractions α_i must therefore sum to one.

$$V_i = \int_V \alpha_i dV \quad \wedge \quad \sum_i \alpha_i = 1 \quad \wedge \quad i \in \{f, s\} \tag{6}$$

Mass conservation is given by

$$\frac{\partial}{\partial t}(\alpha_i \rho_i) + \nabla \cdot (\alpha_i \rho_i u_i) = 0 \tag{7}$$

where the index $i \in \{f, s\}$ and ρ_i and $\mathbf{u}_i$ denote the intrinsic volume averages of density and velocity, respectively.

Both phases obey a general form of the Cauchy momentum transport equation, which for the fluid and solid phase respectively reads

$$\frac{\partial}{\partial t}(\alpha_f \rho_f \mathbf{u}_f) + \nabla \cdot (\alpha_f \rho_f \mathbf{u}_f \mathbf{u}_f) = -\alpha_f \nabla p_f + \nabla \cdot (\alpha_f \boldsymbol{\tau}_f) + \alpha_f \rho_f \mathbf{g} - \frac{1}{V}\sum_{p \in V} \mathbf{f}_j, \tag{8}$$

$$\frac{\partial}{\partial t}(\alpha_s \rho_s \mathbf{u}_s) + \nabla \cdot (\alpha_s \rho_s \mathbf{u}_s \mathbf{u}_s) = -\alpha_s \nabla p_f - \nabla p_s + \nabla \cdot \boldsymbol{\tau}_s + \alpha_s \rho_s \mathbf{g} + \frac{1}{V}\sum_{p \in V} \mathbf{f}_j, \tag{9}$$

where $\boldsymbol{\tau}_i$ is the phasic deviatoric stress tensor comprising some constitutive equation, here a compressible Generalized Newtonian Fluid (GNF) and phase-dependent material functions for the shear and bulk viscosities, η_i and κ_i,

$$\boldsymbol{\tau}_i = 2\eta_i \mathbf{D}_i + \left(\kappa_i - \frac{2}{3}\eta_i\right)(\nabla \cdot \mathbf{u}_i)\mathbf{I}, \tag{10}$$

where $\mathbf{D}_i$ is the symmetric part of the fluid or solid velocity gradient (also known as the rate of deformation tensor, or alternatively the rate of strain tensor)

$$\mathbf{D}_i = \frac{1}{2}\left(\nabla \mathbf{u}_i + \nabla \mathbf{u}_i^T\right) \tag{11}$$

and the shear rate $\dot{\gamma}_i$ is the magnitude of the rate of deformation tensor $\mathbf{D}_i$,

$$\dot{\gamma}_i = \sqrt{2D_i : D_i} \tag{12}$$

The closures for the granular phase are provided in section A.3 and the rheological closures of the fluid are provided in section A.2.

As we are not solving these balance equations to the smallest length scales of the flow, the phenomenon of turbulence is to be modeled. Performing Reynolds averaging (Reynolds, 1895) of the instantaneous balance equations for mass and momentum, a so-called Reynolds stress term $\nabla \cdot (-\rho \overline{\mathbf{u}`\mathbf{u}`})$ arises in the now ensemble-averaged momentum conservation equation. The Reynolds or turbulent stress tensor $\boldsymbol{\tau}_{i,t} = -\rho_i \overline{\mathbf{u}_i` \mathbf{u}_i`}$ is usually assumed symmetric and may be modeled by applying the Boussinesque (1877) hypothesis, also known as the gradient diffusion hypothesis, to relate the Reynolds stresses to the mean velocity gradients and the turbulent viscosity in the form of

$$\tau_{i,t} = -2\mu_{i,t} D_i \tag{13}$$

The employed closures for the turbulent (or eddy) viscosity $\mu_{i,t}$ used in the constitutive equation for the turbulent stress tensor $\boldsymbol{\tau}_{i,t}$ are further detailed in section A.4.

The last terms in equations (8) and (9) are representing the momentum transfer of one phase to the other, where the force sum is to be taken over all particles in the volume V. We here only consider the drag force $\mathbf{f}_D$, which is typically modeled based on the relative velocity

$$\mathbf{u}_r = \mathbf{u}_s - \mathbf{u}_f \tag{14}$$

as

$$\frac{1}{V}\sum_{p \in V} \mathbf{f}_j = K \mathbf{u}_r, \tag{15}$$

To model the interphase exchange coefficient K, we apply the formulation of Gidaspow et al. (1992), which is a combination of the Wen and Yu (1966) model and the Ergun (1952) equation, where the interphase exchange coefficient K is given as

[6] Note that the solid phase may feature some closure law which accounts for the compressibility of granular matter.

$$\alpha_s \leq 0.2: \quad K = c_D \frac{3\alpha_s \rho_f \|\mathbf{u}_r\|}{4\alpha_f^{0.65} d_s}$$
$$\alpha_s > 0.2: \quad K = 150\frac{\alpha_s^2 \eta_f}{\alpha_f d_s^2} + 1.75\frac{\alpha_s \rho_f \|\mathbf{u}_r\|}{d_s} \tag{16}$$

with the coefficient of drag described as

$$c_D = \frac{24}{\alpha_f \mathrm{Re}_p}\left(1 + 0.15(\alpha_f \mathrm{Re}_p)^{0.687}\right), \tag{17}$$

and the particle Reynolds number defined as

$$\mathrm{Re}_p = \frac{\rho_f d_s \|u_r\|}{\eta_f} \tag{18}$$

Appendix A.2. Rheological closures of the fluid phase

We are here concerned with either Newtonian (constant viscosity, e.g. $\eta_f = 0.001002$ Pa s for water) or purely shear-thinning fluids which obey the GNF constitutive equation (10) with $\kappa_f = 0$ assuming incompressibility. In case of shear-thinning fluids the most simple formulation of the viscosity η_f accounting for shear-thinning behavior is the Ostwald (1925) material function, also known as power law (PL),

$$\eta_f(\dot{\gamma}) = K_{PL}\dot{\gamma}^{n_{PL}-1} \tag{19}$$

Drilling fluids may feature a yield stress and are therefore typically described with the Herschel and Bulkley (1926) material function, also known as Yield Power Law (YPL). However, we here limit ourselves to PL fluids as the experimental data used for SP validation is based on a PL fluid.

Appendix A.3. Rheological closures of the solid phase

If the TFM-KTGF framework is used to describe dense granular flows, the entire solid stress tensor, namely equation (10) with index s and including the solid pressure p_s, is given by the sum of collisional/kinetic and frictional components (Savage, 1983)

$$T_s = T_{s,k/c} + T_{s,f} = \sum_{j\in\{k/c,\ f\}}\left[\left(-p_{s,j} + \left(\kappa_{s,j} - \frac{2}{3}\eta_{s,j}\right)\nabla\cdot u_s\right)I + 2\eta_{s,j}D_s\right] \tag{20}$$

Even though the general stencil is that of a compressible Newtonian fluid, namely equation (10), the rheological properties of the solid phase given by the respective material functions as summarized in Table 5 are highly non-linear as they depend on a variety of variables.

Table 5
Overview of solid phase state equations and material functions used to model the kinetic/collisional (index k/c) and frictional (index f) regimes.

Regime	Quantity	Equation	Source
Kinetic and collisional ($j = k/c$)	Pressure	$p_{s,k/c} = \alpha_s\rho_s\Theta_s + 2\alpha_s^2\rho_s\Theta_s(1+e_{ss})g_{0,ss}$ (21)	Lun et al. (1984)
	Shear viscosity	$\eta_{s,c} = \frac{4}{5}\alpha_s^2\rho_s d_s g_{0,ss}(1+e_{ss})\left(\frac{\Theta_s}{\pi}\right)^{\frac{1}{2}}$ (22)	Lun et al. (1984)
	Shear viscosity	$\eta_{s,k} = \frac{10\rho_s d_s\sqrt{\Theta_s\pi}}{96(1+e_{ss})g_{0,ss}}\left(1+\frac{4}{5}\alpha_s(1+e_{ss})g_{0,ss}\right)^{\frac{1}{2}}$ (23)	Gidaspow et al. (1992)
	Bulk viscosity	$\kappa_{s,c/k} = \frac{4}{3}\alpha_s^2\rho_s d_s g_{0,ss}(1+e_{ss})\left(\frac{\Theta_s}{\pi}\right)^{\frac{1}{2}}$ (24)	Lun et al. (1984)
Frictional ($j = f$)	Pressure	$p_{s,f} = 0.05\frac{(\alpha_s - \alpha_{s,f})^2}{(\alpha_{s,mpd} - \alpha_s)^5}$ (25)	Johnson and Jackson (1987)
	Shear viscosity	$\eta_{s,f} = \frac{p_s \sin\varphi_s}{\sqrt{2}\|\mathbf{D}_s\|}$ (26)	Schaeffer (1987)
	Bulk viscosity	n/a	n/a

For instance, for vanishing shear rates in the frictional regime, a

Bingham-type flow behavior is obtained due to the yield feature inherent in equation (26). The kinetic/collisional closures given in Table 5 are functions of the granular temperature Θ_s as a measure for the degree of random particle motion, for which the transport equation reads (Ding and Gidaspow, 1990)

$$\frac{3}{2}\left[\frac{\partial}{\partial t}(\alpha_s\rho_s\Theta_s)+\nabla\cdot(\alpha_s\rho_s u_s\Theta_s)\right]=T_s:\nabla u_s+\nabla\cdot(k_{\Theta_s}\nabla\Theta_s)-D_{\Theta_s}+K_{fs} \tag{27}$$

where k_{Θ_s} is the granular conductivity (e.g. Syamlal et al., 1993) and the granular temperature Θ_s, a measure for the granular fluctuations due to individual particle collisions, is defined as

$$\Theta_s=\frac{1}{3}\langle u_{s,i}^{'}u_{s,i}^{'}\rangle \tag{28}$$

Here, $u_{s,i}$' is the i -th fluctuating component of the solids velocity in the Cartesian coordinate system and the bracket represents an ensemble average of the fluctuating velocities of all particles within a finite volume and time period (Ding and Gidaspow, 1990).

The partial differential equation (21) can be simplified to an algebraic equation by neglecting the convection and diffusion terms – an often used assumption in dense, slow moving fluidized beds, where the local generation and dissipation of granular temperature far outweigh the transport by convection and diffusion. The two final terms in equation (21) are the collisional dissipation of energy (Lun et al., 1984) and the interphase exchange between the particle fluctuations and the liquid phase (Gidaspow et al., 1992).

In equations (21)-(24), $e_{ss}=0.9$ is the coefficient of restitution for particle collisions and

$$g_{0,ss}=\left[1-\left(\frac{\alpha_s}{\alpha_{s,\max}}\right)^{\frac{1}{3}}\right]^{-1} \tag{29}$$

is the radial distribution function accounting for the probability of particle collisions, which has been used frequently in the history of granular flows (Bagnold, 1954; Lun et al., 1984; Ogawa et al., 1980; Sinclair and Jackson, 1989) in the form presented in equation (23).

Appendix A.4. Turbulence closures

Concerning the fluid phase, we here use the Shear Stress Transport (SST) k - ω model (Menter, 1994, 1993), because of its suitability for swirling flows, the possibility to either integrate it to the laminar sublayer or apply wall functions, and because it correctly collapses to the laminar solution in case of laminar flows.

Dropping the fluid index f, the turbulent viscosity is defined as

$$\mu_t=l\frac{\rho k}{\omega} \tag{30}$$

where l is a limiter coefficient ensuring that overprediction of the turbulent viscosity is avoided and therefore enabling the SST k - ω model to better predict the onset and amount of flow separation from smooth surfaces.

The two transport equations for the turbulent kinetic energy k and the specific dissipation ω are

$$\frac{\partial}{\partial t}(\rho k)+\frac{\partial}{\partial x_i}(\rho k u_i)=\frac{\partial}{\partial x_j}\left[\left(\mu+\frac{\mu_t}{\sigma_k}\right)\frac{\partial k}{\partial x_j}\right]+G_k-Y_k \tag{31}$$

and

$$\frac{\partial}{\partial t}(\rho\omega)+\frac{\partial}{\partial x_i}(\rho\omega u_i)=\frac{\partial}{\partial x_j}\left[\left(\mu+\frac{\mu_t}{\sigma_\omega}\right)\frac{\partial\omega}{\partial x_j}\right]+G_\omega-Y_\omega+D_\omega \tag{32}$$

where σ_i are the respective turbulent Prandtl numbers, G_i are respective production terms, Y_i are respective dissipation terms and D_ω is a cross diffusion term, which arises in equation (26) as a consequence of the blending of the standard k - ω model and the standard k - ε model (converted to a k - ω formulation). For further details as well as all relevant closures of the model, the reader is referred to Menter (1994, 1993).

The solid phase turbulence is also described with a turbulent viscosity, i.e. equation (13). However, the turbulence quantities of the solid phase are

obtained from the fluid phase by applying the Tchen theory of dispersion of discrete particles by homogenous turbulence.as given by Simonin and Viollet (1990).

To our knowledge, no non-Newtonian modifications—for instance in the form of damping functions as for the k - ε model (Malin, 1997) or in the form of additional closures for averaged apparent viscosity and turbulent cross-correlations with fluctuating viscosity as a consequence of Reynolds-averaging of the non-constant viscosity (Gavrilov and Rudyak, 2016)—have so far been developed for the k - ω family of models. Hence, we employ the SST k - ω model as implemented in Fluent, and some inaccuracy is expected in the case of non-Newtonian liquids.

Appendix B. CFD velocity field plots

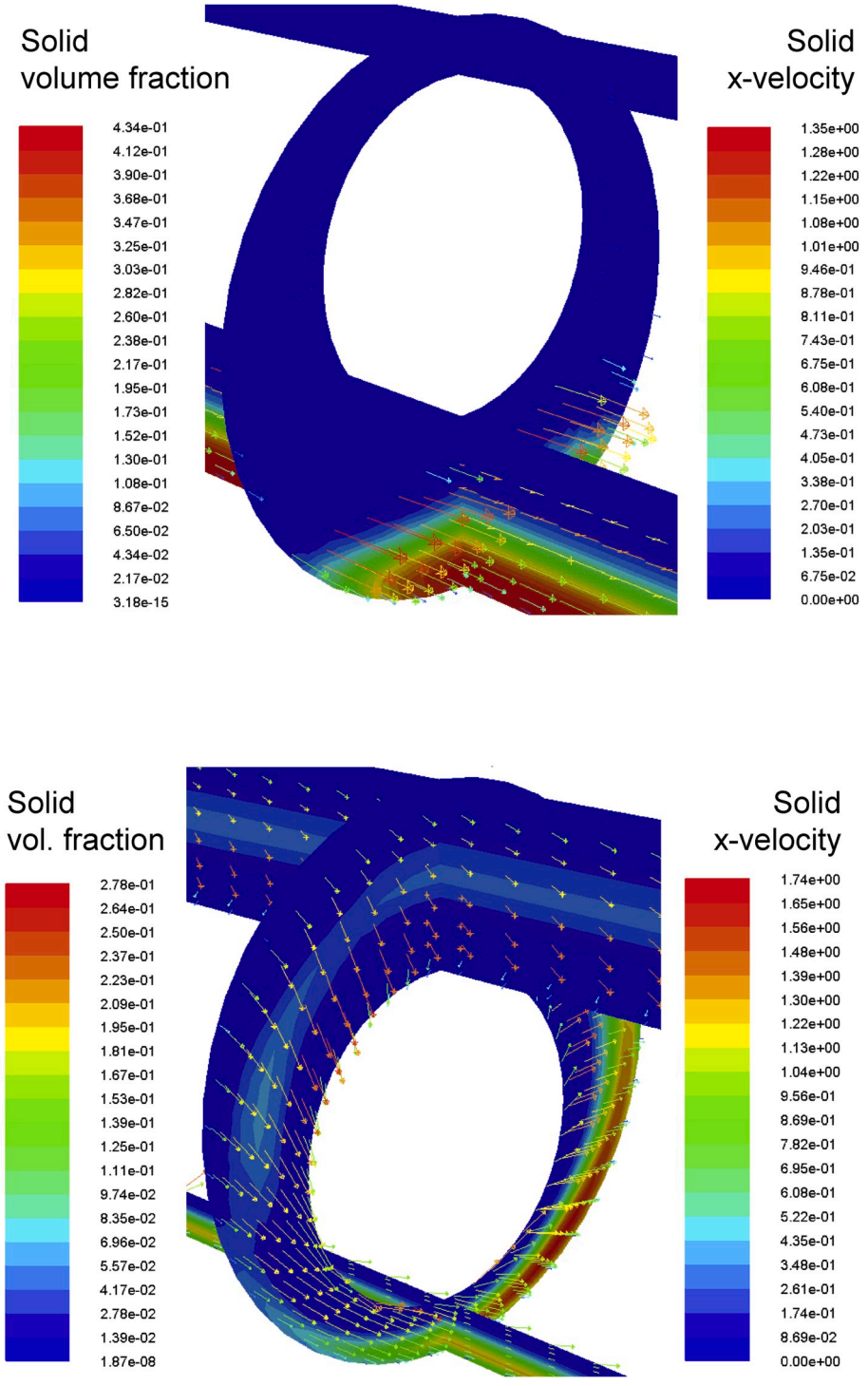

Fig. 15. α_s and $\boldsymbol{u}_s$ fields for e+ (top) and SW (bottom, lower drill pipe position depicted, full video available at https://youtu.be/vw4LUL3dF-c), H2O, $dp/\,dx = -500$ Pa/m and 130 rpm.

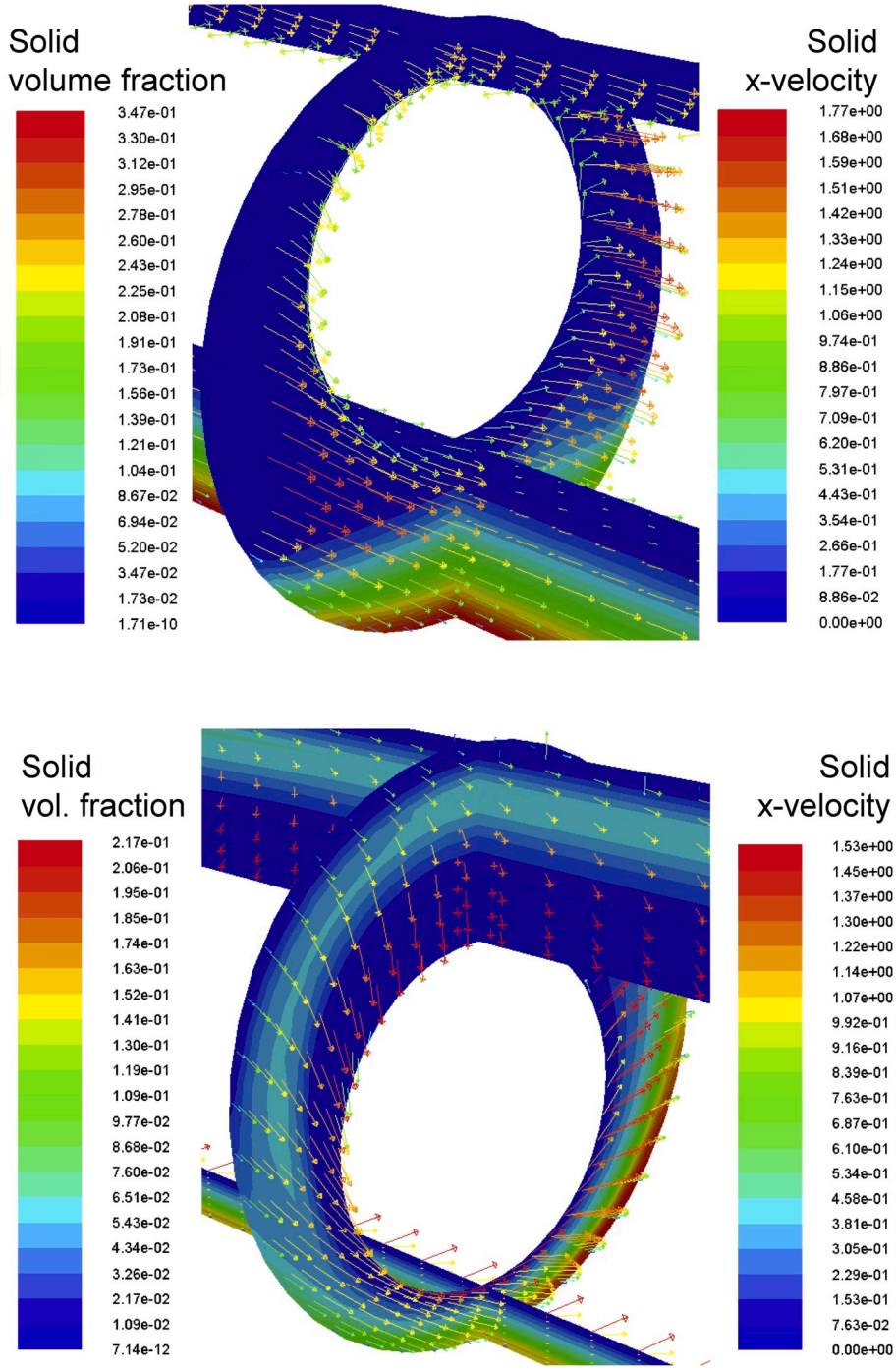

Fig. 16. α_s and $\boldsymbol{u}_s$ fields for e+ (top) and SW (bottom, lower drill pipe position depicted, full video available at https://youtu.be/bbkj9hh8rYw), PAC, $dp/\,dx = -500$ Pa/m and 130 rpm.

Appendix C. Experimental data

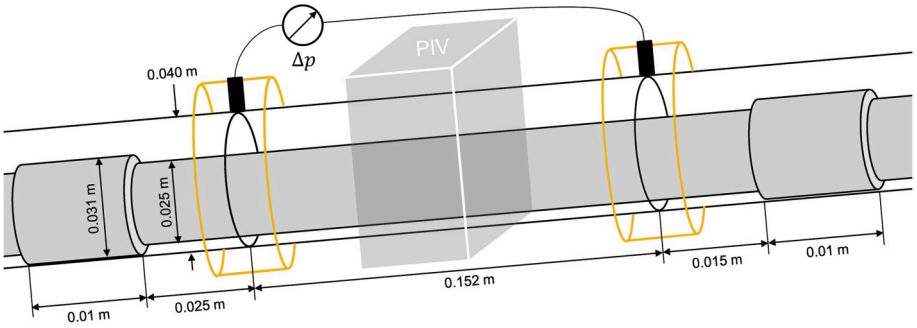

Fig. 17. Annular test section of (Khatibi et al., 2018a, 2018b).

Table 6
Eccentricity E_y and amplitude A_y as observed by (Khatibi et al., 2018a, 2018b) and courtesy of Khatibi (2018).

Q_f [m^3/s]	U_{sf} [m/s]	*rpm* [1/min]	E_y [m]	A_y [m]	$E_y + A_y$ [m]	e_{max} [-]	e_{min} [-]
0.000E+00	0.0000	0.0000	−0.0071	0.0000	−0.0071	−0.94	−0.94
0.000E+00	0.0000	100.0000	−0.0065	0.0046	−0.0019	−0.86	−0.25
0.000E+00	0.0000	200.0000	−0.0058	0.0038	−0.0020	−0.78	−0.27
0.000E+00	0.0000	300.0000	−0.0045	0.0016	−0.0028	−0.60	−0.38
2.600E-04	0.3395	0.0000	−0.0069	0.0000	−0.0069	−0.93	−0.93
2.600E-04	0.3395	100.0000	−0.0064	0.0041	−0.0023	−0.85	−0.31
2.600E-04	0.3395	200.0000	−0.0057	0.0043	−0.0014	−0.76	−0.18
2.600E-04	0.3395	300.0000	−0.0042	0.0022	−0.0020	−0.56	−0.27
4.100E-04	0.5354	0.0000	−0.0069	0.0000	−0.0069	−0.93	−0.93
4.100E-04	0.5354	100.0000	−0.0064	0.0038	−0.0026	−0.85	−0.34
4.100E-04	0.5354	200.0000	−0.0050	0.0027	−0.0023	−0.67	−0.31
4.100E-04	0.5354	300.0000	n/a	n/a	n/a	n/a	n/a
9.400E-04	1.2275	0.0000	−0.0061	0.0000	−0.0061	−0.82	−0.82
9.400E-04	1.2275	100.0000	−0.0056	0.0035	−0.0020	−0.74	−0.27
9.400E-04	1.2275	200.0000	n/a	n/a	n/a	n/a	n/a
9.400E-04	1.2275	300.0000	n/a	n/a	n/a	n/a	n/a

Appendix D. Flow regimes

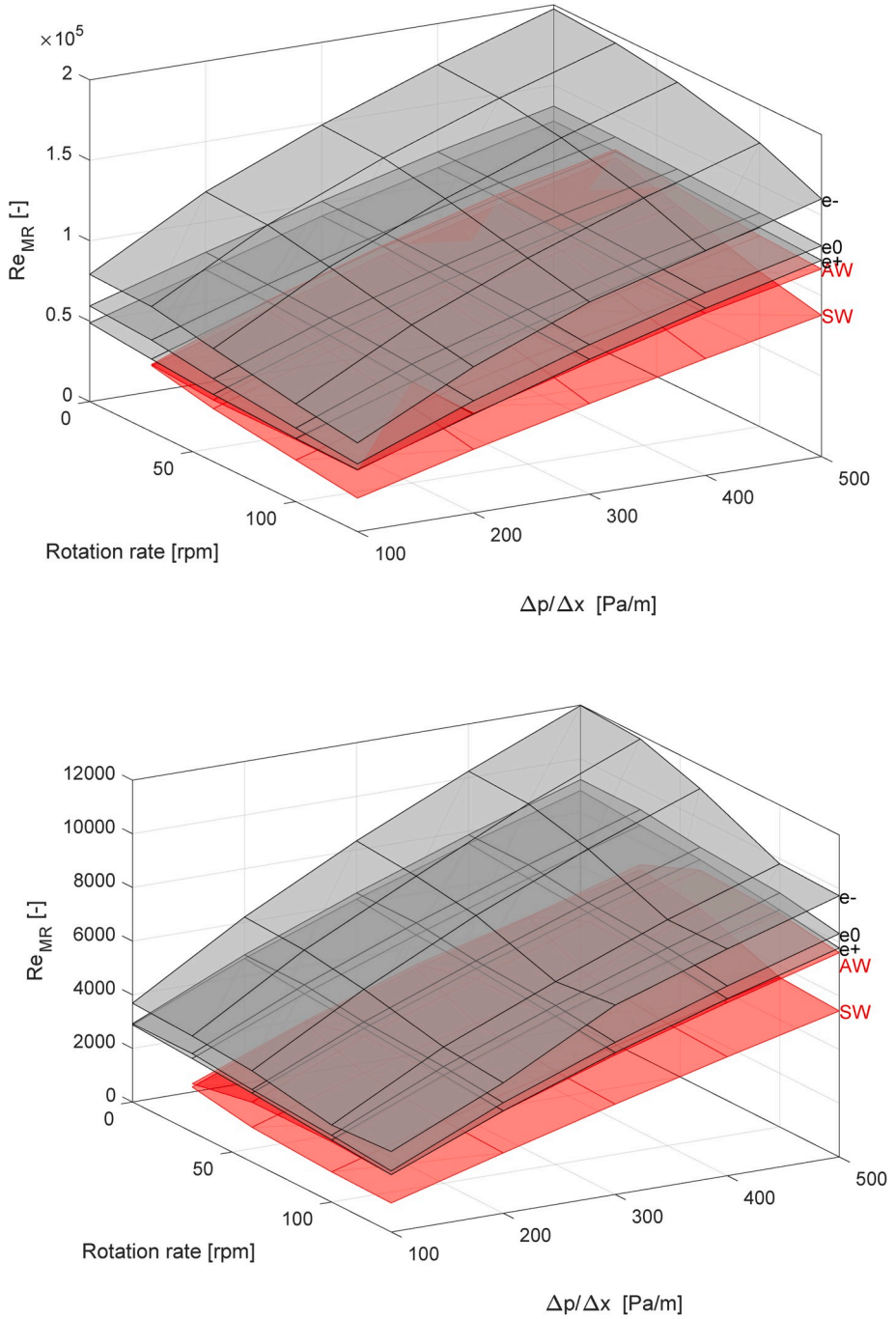

Fig. 18. Metzner and Reed (1955) Reynolds number vs. drill pipe rotation rate and pressure gradient for H2O (top) and PAC (bottom). See Table 3 and Fig. 3 for the test matrix and the system definition, respectively.

Appendix E. Mesh dependence

Table 7
Parameters of the different meshes ($d_i = 0.127$ m, $d_o = 0.216$ m, $L = 0.1$ m $e_y = e_z = 0$) used for the mesh dependency investigation. The coarse mesh is a so-called high Reynolds number mesh where wall functions are used, the superfine mesh is a so-called low Reynolds number mesh, where the wall layer is fully resolved.

	Coarse (High Re)	Intermediate (SP)	Intermediate (MP)	Fine	Superfine (Low Re)
Cells in x-direction	5	10	32	20	40
Cells in r-direction	5	10	10	20	40
Cells in θ-direction	20	40	40	40	160
Δx [m]	0.0200	0.0100	0.0203	0.0050	0.0025
Δr [m]	0.0089	0.0045	0.0045	0.0022	0.0011

(*continued on next page*)

Table 7 (*continued*)

	Coarse (High Re)	Intermediate (SP)	Intermediate (MP)	Fine	Superfine (Low Re)
$\Delta\theta$ [m]	0.0269	0.0135	0.0135	0.0135	0.0034
1st layer height [m]	0.0075	0.002	0.001	0.00085	0.00025
Total cells	500	4000	12800	16000	256000

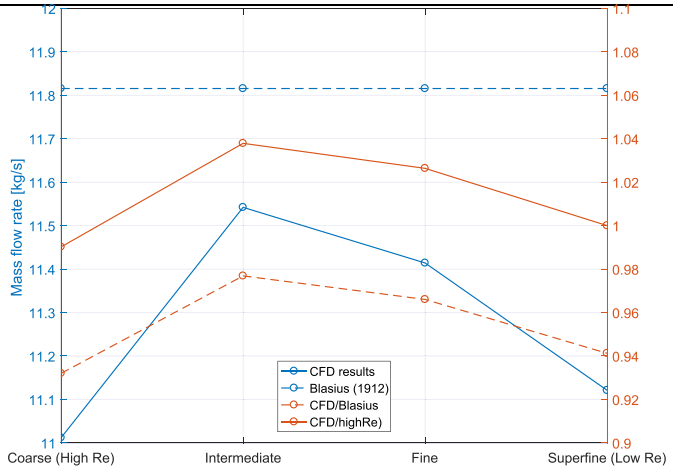

Fig. 19. Mesh dependency of SP water flow (no rotation) for the meshes defined in Table 7 and a pressure difference of $\Delta p/\Delta x = 30$ Pa/m. When comparing the CFD results to the Blasius friction factor correlation, the difference is in the order of −3 … -6% (dashed brown curve). When comparing the simulation results to the low Reynolds number superfine mesh where the wall layer is fully resolved, the difference is in the order of −1 … 4% (solid brown curve). (For interpretation of the references to colour in this figure legend, the reader is referred to the Web version of this article.).

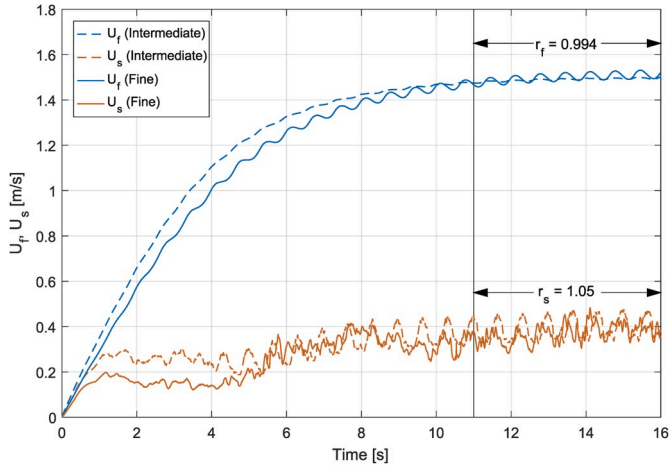

Fig. 20. Mesh dependency of MP water-solid flow for the Coarse and Intermediate meshes defined in Table 7 and a pressure difference of $\Delta p/\Delta x = 500$ Pa. For the time interval 11 … 16 s, the quantity r_i represents the ratio of U_i^{Coarse}/U_i^{Fine}.

References

Agrawal, M., Bakker, A., Prinkey, M.T., 2004. Macroscopic particle model - tracking big particles in CFD. In: The Proceeding of AIChE 2004 Annual Meeting. Presented at the AIChE 2004 Annual Meeting. AIChE, Austin, TX.

Ahmed, R.M., Enfis, M.S., El Kheir, H.M., Laget, M., Saasen, A., 2010. The effect of drillstring rotation on equivalent circulation density: modeling and analysis of field measurements. In: SPE Annual Technical Conference and Exhibition. Presented at the SPE Annual Technical Conference and Exhibition. Society of Petroleum Engineers, Florence, Italy. https://doi.org/10.2118/135587-MS.

Akhshik, S., Behzad, M., Rajabi, M., 2015. CFD–DEM approach to investigate the effect of drill pipe rotation on cuttings transport behavior. J. Petrol. Sci. Eng. 127, 229–244. https://doi.org/10.1016/j.petrol.2015.01.017.

Amanna, B., Khorsand Movaghar, M.R., 2016. Cuttings transport behavior in directional drilling using computational fluid dynamics (CFD). J. Nat. Gas Sci. Eng. 34, 670–679. https://doi.org/10.1016/j.jngse.2016.07.029.

ANSYS, Inc, 2016. ANSYS Fluent User Guide R17.2. ANSYS, Inc., Canonsburg, PA.

ANSYS, Inc, 2016. ANSYS Fluent Theory Guide R17.2. ANSYS, Inc., Canonsburg, PA.

Avila, R.J., Pereira, E.J., Miska, S.Z., Takach, N.E., 2008. Correlations and analysis of cuttings transport with aerated fluids in deviated wells, pp. 132–141. https://doi.org/10.2118/87180-PA. SPE-87180-PA 23.

Bagnold, R.A., 1954. Experiments on a gravity-free dispersion of large solid spheres in a Newtonian fluid under shear. Proc. Roy. Soc. Lond. Math. Phys. Sci. 225, 49–63. https://doi.org/10.1098/rspa.1954.0186.

Bassal, A.A., 1996. The Effect of Drillpipe Rotation on Cuttings Transport in Inclined Wellbores (Master's Thesis). Department of Petroleum Engineering, University of Tulsa.

Bicalho, I.C., dos Santos, D.B.L., Ataíde, C.H., Duarte, C.R., 2016a. Fluid-dynamic behavior of flow in partially obstructed concentric and eccentric annuli with orbital motion. J. Petrol. Sci. Eng. 137, 202–213. https://doi.org/10.1016/j.petrol.2015.11.029.

Bicalho, I.C., Mognon, J.L., Ataíde, C.H., Duarte, C.R., 2016b. Fluid dynamics study of the flow and pressure drop analysis of a non-Newtonian fluid through annular ducts with unusual cross-sections. Can. J. Chem. Eng. 94, 391–401. https://doi.org/10.1002/cjce.22401.

Bilgesu, H.I., Ali, M.W., Aminian, K., Ameri, S., 2002. Computational fluid dynamics (CFD) as a tool to study cutting transport in wellbores. In: Presented at the SPE Eastern Regional Meeting. Society of Petroleum Engineers, Lexington. https://doi.org/10.2118/78716-MS.

Blasius, H., 1912. Das Aehnlichkeitsgesetz bei Reibungsvorgängen. Z. Des. Vereines Dtsch. Ingenieure 19, 639.

Bourgoyne, A.T., Millheim, K.K., Chevenert, M.E., Young Jr., F.S., 1991. Applied Drilling Engineering, second ed. SPE Textbook Series. Society of Petroleum Engineers, Richardson, TX.

Boussinesque, J., 1877. Essai sur la theories des eaux courantes. Tome XXIII (1).

Busch, A., Islam, A., Martins, D., Iversen, F.P., Khatibi, M., Johansen, S.T., Time, R.W., Meese, E.A., 2018a. Cuttings transport modeling - Part 1: specification of benchmark

parameters with a Norwegian continental shelf perspective, 33. SPE Drilling & Completion. https://doi.org/10.2118/180007-PA.
Busch, A., Johansen, S.T., 2018. On the validity of the two-fluid-KTGF approach for dense gravity-driven granular flows. In: Book of Abstracts. Presented at the the 2nd International Symposium on Computational Particle Technology (CPT-2018), CSIRO. Monash University, Melbourne.
Busch, Alexander, Myrseth, V., Khatibi, M., Skjetne, P., Hovda, S., Johansen, S.T., 2018b. Rheological characterization of Polyanionic Cellulose solutions with application to drilling fluids and cuttings transport modeling. Appl. Rheol. 28, 1–16. https://doi.org/10.3933/ApplRheol-28-25154.
Busch, A., Werner, B., Johansen, S.T., 2019. Cuttings transport modeling - Part 2: dimensional analysis and scaling. SPE Drilling & Completion Preprint. https://doi.org/10.2118/198907-PA.
Cayeux, E., Skadsem, H.J., Carlsen, L.A., Stokland, L.M., Cruikshank, S., 2018. Analysis of asymmetric tool-joint wear while drilling long horizontal sections. In: SPE Norway One Day Seminar. Presented at the SPE Norway One Day Seminar. Society of Petroleum Engineers, Bergen, Norway. https://doi.org/10.2118/191339-MS.
Çengel, Y.A., Cimbala, J.M., 2006. Fluid mechanics: fundamentals and applications, McGraw-Hill Series in Mechanical Engineering. McGraw-HillHigher Education, Boston.
Demiralp, Y., 2014. Effects of Drill-Pipe Whirling Motion on Cuttings Transport Performance for Horizontal Drilling. Master Thesis. Lousiana State University.
Ding, J., Gidaspow, D., 1990. A bubbling fluidization model using kinetic theory of granular flow. AIChE J. 36, 523–538. https://doi.org/10.1002/aic.690360404.
Dodge, D.W., Metzner, A.B., 1959. Turbulent flow of non-Newtonian systems. AIChE J. 5, 189–204. https://doi.org/10.1002/aic.690050214.
Dosunmu, I.T., Shah, S.N., 2015. Friction pressure prediction for annular flow of power law fluids. Chem. Eng. Commun. 202, 1380–1388. https://doi.org/10.1080/00986445.2014.938806.
Duan, M., Miska, S., Yu, M., Takach, N.E., Ramadan, A., Hallman, J.H., 2010. Experimental study and modeling of cuttings transport using foam with drillpipe rotation. SPE Drill. Complet. 25 https://doi.org/10.2118/116300-PA.
Duan, M., Miska, S.Z., Yu, M., Takach, N.E., Ramadan, A., Zettner, C.M., 2008. Transport of small cuttings in extended-reach drilling. SPE Drill. Complet. 23 https://doi.org/10.2118/104192-PA.
Epelle, E.I., Gerogiorgis, D.I., 2017. Transient and steady state analysis of drill cuttings transport phenomena under turbulent conditions. Chem. Eng. Res. Des. https://doi.org/10.1016/j.cherd.2017.11.023.
Erge, O., Ozbayoglu, E.M., Miska, S., Yu, M., Takach, N., Saasen, A., May, R., 2015. The effects of drillstring-eccentricity, -rotation, and -buckling configurations on annular frictional pressure losses while circulating yield-power-law fluids. SPE Drill. Complet. 30, 257–271. https://doi.org/10.2118/167950-PA.
Erge, O., Ozbayoglu, E.M., Miska, S.Z., Yu, M., Takach, N., Saasen, A., May, R., 2014. The effects of drillstring eccentricity, rotation, and buckling configurations on annular frictional pressure losses while circulating yield power law fluids. In: SPE-167950-MS. Society of Petroleum Engineers. https://doi.org/10.2118/167950-MS. SPE.
Ergun, S., 1952. Fluid flow through packed columns. Chem. Eng. Prog. 48, 89–94.
Escudier, M.P., Oliveira, P.J., Pinho, F.T., 2002. Fully developed laminar flow of purely viscous non-Newtonian liquids through annuli, including the effects of eccentricity and inner-cylinder rotation. Int. J. Heat Fluid Flow 23, 52–73. https://doi.org/10.1016/S0142-727X(01)00135-7.
Feng, S., Li, Q., Fu, S., 2007. On the orbital motion of a rotating inner cylinder in annular flow. Int. J. Numer. Methods Fluid. 54, 155–173. https://doi.org/10.1002/fld.1388.
Gao, G., 2010. Dynamic buckling and snaking motion of rotating drilling pipe in a horizontal well. SPE J. 11.
Gavrilov, A.A., Rudyak, V.Y., 2016. Reynolds-averaged modeling of turbulent flows of power-law fluids. J. Non-Newtonian Fluid Mech. 227, 45–55. https://doi.org/10.1016/j.jnnfm.2015.11.006.
Gidaspow, D., Bezburuah, R., Ding, J., 1992. Hydrodynamics of circulating fluidized beds: kinetic theory approach. In: Fluidization VII, Proceedings of the 7th Engineering Foundation Conference on Fluidization. Presented at the 7th International Conference on Fluidization, Gold Coast.
Goldschmidt, M.J.V., Beetstra, R., Kuipers, J.A.M., 2004. Hydrodynamic modelling of dense gas-fluidised beds: comparison and validation of 3D discrete particle and continuum models. Powder Technol. 142, 23–47. https://doi.org/10.1016/j.powtec.2004.02.020.
Haaland, S.E., 1983. Simple and explicit formulas for the friction factor in turbulent pipe flow. J. Fluid Eng. 105, 89–90. https://doi.org/10.1115/1.3240948.
Haciislamoglu, M., Cartalos, U., 1994. Practical pressure loss predictions in realistic annular geometries. In: SPE-28304-MS. Society of Petroleum Engineers. https://doi.org/10.2118/28304-MS. SPE.
Haciislamoglu, M., Langlinais, J., 1990. Non-Newtonian flow in eccentric annuli. J. Energy Resour. Technol. 112, 163–169. https://doi.org/10.1115/1.2905753.
Hajidavalloo, E., Sadeghi-Behbahani-Zadeh, M., Shekari, Y., 2013. Simulation of gas–solid two-phase flow in the annulus of drilling well. Chem. Eng. Res. Des. 91, 477–484. https://doi.org/10.1016/j.cherd.2012.11.009.
Han, S.M., Hwang, Y.K., Woo, N.S., Kim, Y.J., 2010. Solid-liquid hydrodynamics in a slim hole drilling annulus. J. Petrol. Sci. Eng. 70, 308–319. https://doi.org/10.1016/j.petrol.2009.12.002.
Herschel, W.H., Bulkley, R., 1926. Konsistenzmessungen von Gummi-benzollösungen. Kolloid Z. 39, 291–300. https://doi.org/10.1007/BF01432034.
Heydari, O., Sahraei, E., Skalle, P., 2017. Investigating the impact of drillpipe's rotation and eccentricity on cuttings transport phenomenon in various horizontal annuluses using computational fluid dynamics (CFD). J. Petrol. Sci. Eng. 156, 801–813. https://doi.org/10.1016/j.petrol.2017.06.059.
Irvine, T.F., 1988. A generalized Blasius equation for power law fluids. Chem. Eng. Commun. 65, 39–47. https://doi.org/10.1080/00986448808940242.
Iversen, F.P., Islam, A., 2018. Hole Cleaning/Cuttings Transport Workshop Meeting Summary. Equinor, Stavanger.
Johansen, S.T., Mo, S., 2015. Improved Fluid Control by Proper Non-newtonian Flow Modeling. Presented at the Tekna Flow Assurance, Larvik.
Johansen, S.T., Skalle, P., Sveen, J., 2003. A generic model for calculation of frictional losses in pipe and annular flows. J. Can. Petrol. Technol. 42 https://doi.org/10.2118/03-06-01.
Johnson, P.C., Jackson, R., 1987. Frictional–collisional constitutive relations for granular materials, with application to plane shearing. J. Fluid Mech. 176, 67–93. https://doi.org/10.1017/S0022112087000570.
Kamyab, M., Rasouli, V., 2016. Experimental and numerical simulation of cuttings transportation in coiled tubing drilling. J. Nat. Gas Sci. Eng. 29, 284–302. https://doi.org/10.1016/j.jngse.2015.11.022.
Kelessidis, V.C., Dalamarinis, P., Maglione, R., 2011. Experimental study and predictions of pressure losses of fluids modeled as Herschel–Bulkley in concentric and eccentric annuli in laminar, transitional and turbulent flows. J. Petrol. Sci. Eng. 77, 305–312. https://doi.org/10.1016/j.petrol.2011.04.004.
Kelin, W., Tie, Y., Xiaofeng, S., Shuai, S., Shizhu, L., 2013. Review and analysis of cuttings transport in complex structural wells. Open Fuel Energy Sci. J. 6, 9–17. https://doi.org/10.2174/1876973X20130610001.
Khatibi, M., 2018. Personal Communication.
Khatibi, M., Time, R.W., Shaibu, R., 2018a. Dynamical feature of particle dunes in Newtonian and shear-thinning flows: relevance to hole-cleaning in pipe and annulus. Int. J. Multiphas. Flow 99, 284–293. https://doi.org/10.1016/j.ijmultiphaseflow.2017.10.015.
Khatibi, M., Wiktorski, E., Sui, D., Time, R.W., 2018b. Experimental study of frictional pressure loss for eccentric drillpipe in horizontal wells. In: SPE-191046-MS. Presented at the IADC/SPE Asia Pacific Drilling Technology Conference and Exhibition. Society of Petroleum Engineers, SPE, p. 18. https://doi.org/10.2118/191046-MS.
Larsen, T.I.F., 1990. A Study of the Critical Fluid Velocity in Cuttings Transport for Inclined Wellbores (Master). Department of Petroleum Engineering, University of Tulsa, Tulsa.
Leine, R.I., van Campen, D.H., Keultjes, W.J.G., 2002. Stick-slip whirl interaction in drillstring dynamics. J. Vib. Acoust. 124, 209. https://doi.org/10.1115/1.1452745.
Leonard, B.P., 1979. A stable and accurate convective modelling procedure based on quadratic upstream interpolation. Comput. Methods Appl. Mech. Eng. 19, 59–98.
Li, J., Luft, B., 2014a. Overview of Solids Transport Studies and Applications in Oil and Gas Industry. In: Experimental Work. Presented at the SPE Russian Oil and Gas Exploration & Production Technical Conference and Exhibition. Society of Petroleum Engineers, Moscow. https://doi.org/10.2118/171285-MS.
Li, J., Luft, B., 2014b. Overview Solids Transport Study and Application in Oil-Gas Industry - Theoretical Work. In: Presented at the International Petroleum Technology Conference, International Petroleum Technology Conference, Kuala Lumpur. https://doi.org/10.2523/IPTC-17832-MS.
Lien, K., Monty, J.P., Chong, M.S., Ooi, A., 2004. The entrance length for fully developed turbulent channel flow. In: Presented at the 15th Australasian Fluid Mechanics Conference. The University of Sydney, Sydney, p. 4.
Lun, C.K.K., Savage, S.B., Jeffrey, D.J., Chepurniy, N., 1984. Kinetic theories for granular flow: inelastic particles in Couette flow and slightly inelastic particles in a general flowfield. J. Fluid Mech. 140, 223–256. https://doi.org/10.1017/S0022112084000586.
Malin, M.R., 1997. Turbulent pipe flow of power-law fluids. Int. Commun. Heat Mass Tran. 24, 977–988. https://doi.org/10.1016/S0735-1933(97)00083-3.
McCann, R.C., Quigley, M.S., Zamora, M., Slater, K.S., 1995. Effects of high-speed pipe rotation on pressures in narrow annuli. SPE Drill. Complet. 10 https://doi.org/10.2118/26343-PA.
Menter, F.R., 1994. Two-equation eddy-viscosity turbulence models for engineering applications. AIAA J. 32, 1598–1605. https://doi.org/10.2514/6.1993-2906.
Menter, F.R., 1993. Zonal Two Equation K-ω Turbulence Models for Aerodynamic Flows. In: Presented at the 24th Fluid Dynamics Conference. American Institute of Aeronautics and Astronautics (AIAA), Orlando, Florida, p. 22.
Metzner, A.B., Reed, J.C., 1955. Flow of non-Newtonian fluids-correlation of the laminar, transition, and turbulent-flow regions. AIChE J. 1, 434–440. https://doi.org/10.1002/aic.690010409.
Mme, U., Skalle, P., 2012. CFD calculations of cuttings transport through drilling annuli at various angles. Int. J. Petrol. Sci. Technol. 6, 129–141.
Neto, J.L.V., Martins, A.L., Ataíde, C.H., Barrozo, M.A.S., 2012. Non-Newtonian flows in annuli with variable eccentric motion of the inner tube. Chem. Eng. Technol. 35, 1981–1988. https://doi.org/10.1002/ceat.201200239.
Ofei, T.N., Irawan, S., Pao, W., 2015. Drilling Parameter Effects on Cuttings Transport in Horizontal Wellbores: A Review. In: Awang, M., Negash, B.M., Md Akhir, N.A., Lubis, L.A. (Eds.), ICIPEG 2014. Springer Singapore, Singapore, pp. 199–207. https://doi.org/10.1007/978-981-287-368-2_18.
Ofei, T.N., Irawan, S., Pao, W., 2014. 2014. CFD method for predicting annular pressure losses and cuttings concentration in eccentric horizontal wells. J. Petrol. Eng. 1–16. https://doi.org/10.1155/2014/486423.
Ofei, T.N., Pao, W., 2014. Modelling of pressure drop and cuttings concentration in eccentric narrow horizontal well bore with rotating drillpipe. J. Appl. Sci. 14, 3263–3269. https://doi.org/10.3923/jas.2014.3263.3269.
Ogawa, S., Umemura, A., Oshima, N., 1980. On the equations of fully fluidized granular materials. ZAMP (Z. Angew. Math. Phys.) 31, 483–493. https://doi.org/10.1007/BF01590859.

Ogugbue, C.C., Shah, S., 2011. Laminar and turbulent friction factors for annular flow of drag-reducing polymer solutions in coiled-tubing operations. SPE-130579-PA. https://doi.org/10.2118/130579-PA.
Ostwald, W., 1925. Über die Geschwindigkeitsfunktion der Viskosität disperser Systeme. Colloid Polym. Sci. 36, 99–117.
Pang, B., Wang, S., Jiang, X., Lu, H., 2019. Effect of orbital motion of drill pipe on the transport of non-Newtonian fluid-cuttings mixture in horizontal drilling annulus. J. Petrol. Sci. Eng. 174, 201–215. https://doi.org/10.1016/j.petrol.2018.11.009.
Pang, B., Wang, S., Wang, Q., Yang, K., Lu, H., Hassan, M., Jiang, X., 2018. Numerical prediction of cuttings transport behavior in well drilling using kinetic theory of granular flow. J. Petrol. Sci. Eng. 161, 190–203. https://doi.org/10.1016/j.petrol.2017.11.028.
Peden, J.M., Ford, J.T., Oyeneyin, M.B., 1990. Comprehensive experimental investigation of drilled cuttings transport in inclined wells including the effects of rotation and eccentricity. In: European Petroleum Conference. Society of Petroleum Engineers, The Hague. https://doi.org/10.2118/20925-MS.
Pereira, F. a R., Barrozo, M. a S., Ataide, C.H., 2007. CFD predictions of drilling fluid velocity and pressure profiles in laminar helical flow. Braz. J. Chem. Eng. 24, 587–595. https://doi.org/10.1590/S0104-66322007000400011.
Pilehvari, A., Azar, J.J., Shirazi, S., 1999. State-of-the-art cuttings transport in horizontal wellbores. SPE Drill. Complet. 14 https://doi.org/10.2118/57716-PA.
Pilehvari, A., Serth, R., 2009. Generalized hydraulic calculation method for axial flow of non-newtonian fluids in eccentric annuli. SPE-111514-PA. https://doi.org/10.2118/111514-PA.
Poole, R.J., 2010. Development-length requirements for fully developed laminar flow in concentric annuli. J. Fluid Eng. 132, 4. https://doi.org/10.1115/1.4001694.
Reynolds, O., 1895. On the dynamical theory of incompressible viscous fluids and the determination of the criterion. Phil. Trans. Roy. Soc. Lond. 186, 123–164.
Rooki, R., Ardejani, F.D., Moradzadeh, A., Norouzi, M., 2013a. Cuttings transport modeling in foam drilling using computational fluid dynamics (CFD). Int. J. Petrol. Geosci. Eng. (IJPGE) 1, 115–127.
Rooki, R., Ardejani, F.D., Moradzadeh, A., Norouzi, M., 2013b. Simulation of cuttings transport with foam in deviated wellbores using computational fluid dynamics. J. Petrol. Expl. Prod. Technol. 4, 263–273. https://doi.org/10.1007/s13202-013-0077-7.
Saasen, A., 2014. Annular frictional pressure losses during drilling - predicting the effect of drillstring rotation. J. Energy Resour. Technol. 136, 034501 https://doi.org/10.1115/1.4026205.
Sanchez, R.A., Azar, J.J., Bassal, A.A., Martins, A.L., 1999. Effect of drillpipe rotation on hole cleaning during directional-well drilling. SPE J. 4 https://doi.org/10.2118/56406-PA.
Savage, S.B., 1983. Granular flows down rough inclines - review and extension. In: Studies in Applied Mechanics. Elsevier, pp. 261–282. https://doi.org/10.1016/B978-0-444-42192-0.50028-1.
Savage, S.B., Jeffrey, D.J., 1981. The stress tensor in a granular flow at high shear rates. J. Fluid Mech. 110, 255–272. https://doi.org/10.1017/S0022112081000736.
Savage, S.B., Pfeffer, R., Zhao, Z.M., 1996. Solids transport, separation and classification. Powder Technol. 88, 323–333.
Sayindla, S., Lund, B., Ytrehus, J.D., Saasen, A., 2017. Hole-cleaning performance comparison of oil-based and water-based drilling fluids. J. Petrol. Sci. Eng. 159, 49–57. https://doi.org/10.1016/j.petrol.2017.08.069.
Schaeffer, D.G., 1987. Instability in the evolution equations describing incompressible granular flow. J. Differ. Equ. 66, 19–50.
Shyu, R.-J., 1989. Bending Vibration of Rotating Drill Strings (PhD Thesis). Massachusetts Institute of Technology (MIT).
Sifferman, T.R., Becker, T.E., others, 1992. Hole cleaning in full-scale inclined wellbores. SPE Drill. Eng. 7, 115–120.
Simonin, C., Viollet, P.L., 1990. Predictions of an oxygen droplet pulverization in a compressible subsonic coflowing hydrogen flow. Num. Methods Multiphase Flows FED91, 65–82.
Sinclair, J.L., Jackson, R., 1989. Gas-particle flow in a vertical pipe with particle-particle interactions. AIChE J. 35, 1473–1486. https://doi.org/10.1002/aic.690350908.
Sorgun, M., Aydin, I., Ozbayoglu, M.E., 2011. Friction factors for hydraulic calculations considering presence of cuttings and pipe rotation in horizontal/highly-inclined wellbores. J. Petrol. Sci. Eng. 78, 407–414. https://doi.org/10.1016/j.petrol.2011.06.013.
Syamlal, M., Rogers, W., O'Brien, T.J., 1993. MFIX Documentation Theory Guide. U.S. Department of Energy, Office of Fossil Energy, Morgantown.
Tomren, P.H., Iyoho, A.W., Azar, J.J., 1986. Experimental study of cuttings transport in directional wells. SPE Drill. Eng. 1, 43–56. https://doi.org/10.2118/12123-PA.
Vasquez, S., 2000. A phase coupled method for solving multiphase problems on unstructured mesh. In: Presented at the ASME 200 Fluids Engineering Division Summer Meeting.
Wang, Z., Guo, X., Li, M., Hong, Y., 2009. Effect of drillpipe rotation on borehole cleaning for extended reach well. J. Hydrodynam., Ser. B 21, 366–372. https://doi.org/10.1016/S1001-6058(08)60158-4.
Wen, C.Y., Yu, Y.H., 1966. Mechanics of fluidization. Present. Chem. Eng. Prog., Symp. Ser. 100–111.
Werner, B., 2018. The Influence of Drilling Fluid Rheology on Cuttings Bed Behavior (PhD). Norwegian University of Science and Technology, Trondheim.
Xiao, W., Zhang, Y., Zhong, Y., 2003. Annulus whirling motion analysis of the rotary drill string by the action of hydrodynamic pressure and friction force. In: 19th Biennial Conference on Mechanical Vibration and Noise, Parts A, B, and C. Presented at the ASME 2003 International Design Engineering Technical Conferences and Computers and Information in Engineering Conference, vol. 5. ASME, Chicago, Illinois, USA, pp. 1003–1010. https://doi.org/10.1115/DETC2003/VIB-48423.
Xiaofeng, S., Kelin, W., Tie, Y., 2013. Review of hole cleaning in complex structural wells. Open Petrol. Eng. J. 6, 25–32. https://doi.org/10.2174/1874834101306010025.
Xiaofeng, S., Kelin, W., Tie, Y., Shao, S., Jiao, J., 2014. Effect of drillpipe rotation on cuttings transport using computational fluid dynamics (CFD) in complex structure wells. J. Petrol. Expl. Prod. Technol. 4, 255–261. https://doi.org/10.1007/s13202-014-0118-x.
Ytrehus, J.D., Lund, B., Taghipour, A., Kosberg, B.R., Carazza, L., Gyland, K.R., Saasen, A., 2018. Cuttings bed removal in deviated wells. In: Proceedings of the 37th International Conference on Ocean, Offshore and Arctic Engineering (OMAE2018). Presented at the 37th International Conference on Ocean, Offshore and Arctic Engineering (OMAE2018). American Society of Mechanical Engineers (ASME), Madrid. https://doi.org/10.1115/OMAE2018-77832.
Ytrehus, J.D., Taghipour, A., Sayindla, S., Lund, B., Werner, B., Saasen, A., 2015. Full scale flow loop experiments of hole cleaning performances of drilling fluids. ASME. https://doi.org/10.1115/OMAE2015-41901. V010T11A041.
Zakerian, A., Sarafraz, S., Tabzar, A., Hemmati, N., Shadizadeh, S.R., 2018. Numerical modeling and simulation of drilling cutting transport in horizontal wells. J. Petrol. Expl. Prod. Technol. https://doi.org/10.1007/s13202-018-0435-6.
Zhang, G., Gutierrez, M., Li, M., 2016. A coupled CFD-DEM approach to model particle-fluid mixture transport between two parallel plates to improve understanding of proppant micromechanics in hydraulic fractures. Powder Technol. https://doi.org/10.1016/j.powtec.2016.11.055.